

# Silicon Burning II: Quasi-Equilibrium and Explosive Burning

W. Raphael Hix<sup>1,2,3,4</sup> & Friedrich-Karl Thielemann<sup>3,5</sup>

## ABSTRACT

Having examined the application of quasi-equilibrium to hydrostatic silicon burning in Paper I of this series, Hix & Thielemann (1996), we now turn our attention to explosive silicon burning. Previous authors have shown that for material which is heated to high temperature by a passing shock and then cooled by adiabatic expansion, the results can be divided into three broad categories; *incomplete burning*, *normal freezeout* and  *$\alpha$ -rich freezeout*, with the outcome depending on the temperature, density and cooling timescale. In all three cases, we find that the important abundances obey quasi-equilibrium for temperatures greater than approximately  $3 \times 10^9$  K, with relatively little nucleosynthesis occurring following the breakdown of quasi-equilibrium. We will show that quasi-equilibrium provides better abundance estimates than global nuclear statistical equilibrium, even for normal freezeout and particularly for  $\alpha$ -rich freezeout. We will also examine the accuracy with which the final nuclear abundances can be estimated from quasi-equilibrium.

*Subject headings:* nuclear reactions, nucleosynthesis, abundances — stars: evolution — supernovae: general

## 1. Introduction

Because the products of hydrostatic silicon burning are trapped deep in the potential well of their parent star, it is only by explosion that the interstellar medium is enriched in intermediate mass and iron peak elements. In core collapse supernovae, the neutrino

---

<sup>1</sup>Joint Institute for Heavy Ion Research, Oak Ridge National Laboratory, Oak Ridge, TN 37831-6374

<sup>2</sup>Department of Physics and Astronomy, University of Tennessee, Knoxville, TN 37996-1200

<sup>3</sup>Physics Division, Oak Ridge National Laboratory, Oak Ridge, TN 37831-6373

<sup>4</sup>Department of Astronomy, University of Texas, Austin TX, 78712

<sup>5</sup>Department of Physics and Astronomy, University of Basel, Klingelberstrasse 82, CH-4056 Basel Switzerland

driven shock passes through the silicon and oxygen shells, heating the material and driving at least a portion outward. For thermonuclear supernovae, the degenerate ignition of carbon and oxygen provides both the fuel for silicon burning and the energy required to unbind this material from its parent white dwarf. In both cases, matter is heated rapidly to temperatures sufficient to destroy silicon and expelled outward, to expand and cool adiabatically. Thus, understanding the chemical evolution of the intermediate mass and iron peak elements, and how the formation of these elements affects the supernovae which produce them, requires understanding the behavior of silicon burning under such explosive conditions. Recent calculations of both core collapse and thermonuclear supernovae seem to indicate that, in both cases, silicon burning occurs in material subject to strong hydrodynamic instabilities, prompting two- and ultimately three-dimensional simulations. See, for example, Bazan & Arnett (1994) for discussion of convection prior to core collapse; Herant, Benz, Hix, Fryer & Colgate (1994), Burrows, Hayes & Fryxell (1995), Janka & Müller (1995), and Mezzacappa et al. (1998) for discussion of core collapse instabilities; and Khokhlov (1993), Khokhlov (1995), and Niemeyer & Hillebrandt (1995) for discussion of turbulent flames in thermonuclear supernovae. While it has been possible to perform simulations of silicon burning using large nuclear networks within spherically symmetric models comprised of hundreds of zones, the need to understand silicon burning in these multi-dimensional contexts, with the attendant squaring and cubing of the number of zones, demands more efficient calculation. This provides an additional motivation for our study, as we seek to leverage our understanding of silicon burning to reduce its computational cost.

In a previous paper, Hix & Thielemann (1996), henceforth HT96, we described how the physics of silicon burning is dominated by partial equilibria among groups of nuclei well before complete nuclear statistical equilibrium (NSE) is established. Bodansky, Clayton & Fowler (1968) introduced the concept of quasi-equilibrium (QSE), contending that the solar system abundances of nuclei between neon and the iron peak could be explained by a single quasi-equilibrium group which stretched from magnesium through the iron peak but failed to reach NSE. This mechanism unified the  $\alpha$ - and e-processes of Burbidge, Burbidge, Fowler & Hoyle (1957) and reconciled moderately well with the nuclear network calculations of Truran, Cameron & Gilbert (1966). QSE is a local equilibrium with respect to strong and electromagnetic reactions, i.e. the exchange of neutrons, protons,  $\alpha$ -particles and photons. In HT96, we demonstrated that the abundance of a nucleus in QSE with  $^{28}\text{Si}$ , for example, is given by

$$Y_{QSE}(^AZ) = \left( \frac{C(^AZ)}{C(^{28}\text{Si})} \right) Y(^{28}\text{Si}) Y_n^{N-14} Y_p^{Z-14} , \quad (1)$$

where  $Y_n$ ,  $Y_p$ , and  $Y(^{28}\text{Si})$  are the abundances of free neutrons, free protons, and  $^{28}\text{Si}$ . The thermodynamic conditions and nuclear properties are contained within the expressions

$$C(^AZ) = \frac{G(^AZ)}{2^A} \left( \frac{\rho N_A}{\theta} \right)^{A-1} A^{\frac{3}{2}} \exp \left( \frac{B(^AZ)}{k_B T} \right) \quad (2)$$

which has been defined for later convenience, with

$$\theta = \left( \frac{m_u k_B T}{2\pi\hbar^2} \right)^{3/2} . \quad (3)$$

$G(^AZ)$  and  $B(^AZ)$  are the partition function and binding energy of the nucleus  $^AZ$ ,  $N_A$  is Avagadro’s number,  $k_B$  is Boltzmann’s constant, and  $\rho$  and  $T$  are the density and temperature of the plasma. It is worth noting that, due to the  $\exp(B(^AZ)/k_B T)$  term, declining temperature favors the more tightly bound nuclei. Furthermore, for the thermodynamic conditions common to silicon burning, the nuclear binding energy,  $B(^AZ)$ , must be corrected for the effects of Coulomb screening (Hix, Thielemann, Fushiki & Truran 1999).

As Eq. 1 demonstrates, the abundance of any nucleus in quasi-equilibrium can be expressed as a function of just three abundances, the thermodynamic conditions ( $\rho$ ,  $T_9$ ) and the properties of that nucleus, subsumed here within  $C(^AZ)$ . Thus the evolution of the abundances of  $^{28}\text{Si}$  and the free nucleons defines the behavior of all the nuclei in QSE with  $^{28}\text{Si}$ . One can naturally construct similar equations relative to nuclei other than  $^{28}\text{Si}$ , though for all nuclei within the silicon QSE group, all such equations reduce to Eq. 1. This expression for quasi-equilibrium, Eq. 1, is also identical to those defined by Bodansky, Clayton & Fowler (1968), Woosley, Arnett & Clayton (1973) and Meyer, Krishnan, & Clayton (1996), provided the  $\alpha$ -particles, protons and neutrons are internally in equilibrium. We find that, by the time quasi-equilibrium is established in the vicinity of silicon, these light nuclei consistently have formed their own QSE group, with abundances in this light QSE group obeying the NSE relation (Eq.4). These light nuclei remain in QSE until the bulk of the photodisintegration rates freezeout for  $T_9 \approx 3$ .

In contrast to quasi-equilibrium, nuclear statistical equilibrium is a global equilibrium. From arguments based on chemical potentials or detailed balance of reactions (see, for example, Hix, Thielemann, Fushiki & Truran 1999, Hartmann, Woosley & El Eid 1985, Clayton 1968, 1983, or Clifford & Tayler 1965), an expression for the equilibrium abundances of all nuclei can be derived,

$$Y_{NSE}(^AZ) = C(^AZ) Y_n^N Y_p^Z . \quad (4)$$

Here  $C(^AZ)$  is identical to Eq. 2, and  $Y_n$  and  $Y_p$  are the free neutron and free proton abundances. Thus in NSE, the abundances of all nuclei are functions of only two abundances. Substitution of Eq. 4, evaluated for  $^{28}\text{Si}$ , into Eq. 1, reveals that for all nuclei Eq. 1 reduces to Eq. 4 if  $^{28}\text{Si}$  has reached NSE. Thus failure of a quasi-equilibrium group to reach NSE implies that while the members of the group have achieved equilibrium with respect to the exchange of free nucleons and  $\alpha$ -particles, they have not achieved global equilibrium with the free nucleons.

In HT96, in order to separate the details of silicon burning from the vagaries of hydrodynamics, we considered only constant thermodynamic conditions. Further, we limited ourselves to conditions appropriate for hydrostatic silicon burning in the late stages of stellar evolution. While the thermodynamic variations within the core of a star undergoing hydrostatic silicon burning occur slowly, this is certainly not true for convective or explosive silicon burning. If quasi-equilibrium is to be useful in understanding and simplifying the modeling of silicon burning within a hydrodynamic supernova model, it is necessary to demonstrate that its applicability is not limited to constant conditions. As a representative analytic model for silicon burning occurring as a result of shock heating, we will consider a mass zone which is instantaneously heated by a passing shock to some peak initial temperature,  $T_{9i}$ , and density,  $\rho_i$ , and then expands and cools adiabatically. Following the approximation introduced by Fowler & Hoyle (1964), the expansion timescale (equal to the free fall timescale) is

$$\tau_{\text{HD}} = (24\pi G\rho)^{-1/2} = 446\rho_6^{-1/2}\text{ms}, \quad (5)$$

with the time dependence of the density and temperature of this radiation dominated gas given by

$$\begin{aligned} \rho(t) &= \rho_i \exp(-t/\tau_{\text{HD}}), \\ T_9(t) &= T_{9i} \exp(-t/3\tau_{\text{HD}}), \end{aligned} \quad (6)$$

assuming the adiabatic exponent  $\gamma = 4/3$ . This model provides a strong but simple test of the behavior of quasi-equilibrium under varying conditions.

Previous authors, beginning with Woosley, Arnett & Clayton (1973), have shown that for explosive burning, the  $T_{9i}, \rho_i$  plane is divided into 3 regions. Figure 1 portrays this division for material with  $Y_e \lesssim .5$ , while also showing the remnant helium mass fraction. The squares plotted in this figure indicate the range of conditions found in the W7 model for Type Ia supernovae (see Thielemann, Nomoto, & Yokoi 1986), while the circles show conditions typical for Type II supernovae models (see, for example, Woosley & Weaver 1995 and Thielemann, Nomoto, & Hashimoto 1996). In the first region, roughly defined by  $T_{9i} < 5$ , cooling due to the expansion halts the destruction of silicon prematurely, resulting in a larger remnant concentration of intermediate mass elements than nuclear statistical equilibrium would suggest. Quite naturally, this is referred to as *incomplete silicon burning*. For higher temperatures silicon is exhausted, and NSE is reached before the reactions freeze out. For moderately large densities ( $\rho_i \gtrsim 10^8 \text{ g cm}^{-3}$ ), the abundances of the light QSE group nuclei are relatively small, allowing these light nuclei to pass through the A=5-8 bottleneck and form heavier nuclei as the temperature, and therefore their equilibrium population, drops. When this occurs, NSE persists up until freezeout at  $T_9 \sim 3$ , resulting in a *normal freezeout*. At lower densities the light group nuclei, especially  $^4\text{He}$ , contain

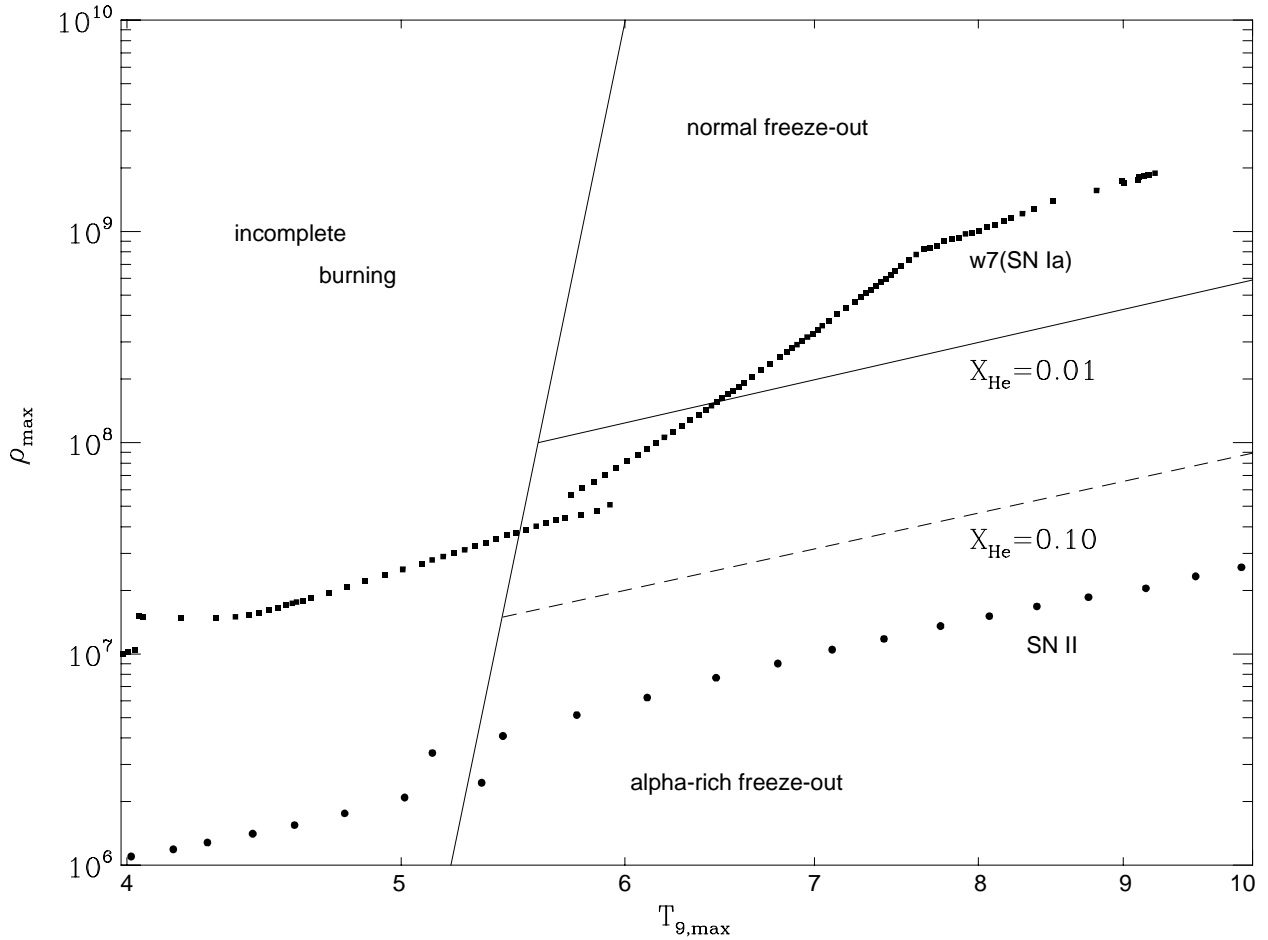


Fig. 1.— Outcome of explosive silicon burning as a function of peak temperature and density. Contour lines of constant  ${}^4\text{He}$  mass fractions in complete burning are given for levels of 1 and 10%. They coincide with lines of constant radiation entropy per gram of matter. For comparison also the maximum  $\rho$ – $T$ -conditions of individual mass zones in type Ia and type II supernovae are indicated.

a large portion of the nuclear mass fraction. This larger NSE abundance of light nuclei, coupled with the reduced reaction flow through the bottleneck due to the quadratic density dependence of the rates for the  $\alpha + \alpha + \alpha \rightarrow {}^{12}\text{C}$  and  $\alpha + \alpha + n \rightarrow {}^9\text{Be}$  reactions which bridge this mass gap, prevents the incorporation of all of these light nuclei into heavier nuclei on the timescale of the cooling. Since the same binding energy considerations which favor the iron peak nuclei in NSE also favor  $\alpha$ -particles over free nucleons, the light group mass is dominated by  $\alpha$ -particles, hence this is termed  *$\alpha$ -rich freezeout*. This paper will analyze and demonstrate the applicability of quasi-equilibrium for each of the 3 results of explosive silicon burning detailed above.

## 2. Incomplete Burning

We begin with incomplete silicon burning and an example where  $T_{9i} = 5$ ,  $\rho = 10^9 \text{ g cm}^{-3}$  and  $Y_e = .48$ . Figure 2a displays the ratio of the network abundances to their silicon QSE abundances plotted as a function of atomic mass after an elapsed time of  $9.6 \times 10^{-7}$  seconds. This figure is reminiscent of the figures discussed in HT96. As in HT96, these QSE abundances are calculated from the network values of  $Y_n$ ,  $Y_p$ , and  $Y(^{28}\text{Si})$ , not on an independent QSE-based calculation. In Figures 2, 3 & 5, the filled triangles, squares and circles mark the core nuclei of the 3 QSE group discussed in that paper. These same 3 QSE groups are clearly present here, one composed of the light nuclei, the second centered on silicon and the third containing the iron peak nuclei. One point to note is the apparent displacement of  $^3\text{He}$  from the light group. We believe that this is due to a limitation of our reaction set, which contains many fewer reactions involving  $^3\text{He}$  than reactions involving  $^4\text{He}$ . If the corresponding reactions for  $^3\text{He}$ , which are important only to the abundance of  $^3\text{He}$ , were included,  $^3\text{He}$  would also be in QSE with the free nucleons. Clearly quasi-equilibrium is well established early in this calculation. We then must ask, Under what conditions does quasi-equilibrium fail to be a good approximation to the network abundances? Figure 2b is similar to Figure 2a, with an elapsed time of  $4.4 \times 10^{-3}$  seconds. By this time,  $T_9$  has dropped to 4.5 and  $\rho = 7.3 \times 10^8 \text{ g cm}^{-3}$ . The evolution of the QSE groups follows the pattern discussed under constant thermodynamic conditions in HT96, with both the light and iron peak groups converging toward the silicon group. In particular, the convergence of the light and silicon QSE groups reflects the approach of the network abundances to those calculated from NSE for the current thermodynamic conditions.

However, as time continues to elapse, this convergence reverses with the network abundances diverging from the then current NSE abundances. As we discussed in §1, in equilibrium, decreasing temperature favors the more bound members of a group of nuclei. In this case, decreasing temperature raises the quasi-equilibrium abundances of the iron peak nuclei relative to all other nuclei. Over this span of time, though the abundances of the iron peak nuclei are increasing, their QSE abundances are increasing more rapidly, moving the iron peak QSE group away from equilibrium with silicon. Similarly, because of the shift in favor of heavier nuclei, though the network abundance of silicon is declining, the equilibrium abundance of silicon is declining more rapidly, leaving silicon further from equilibrium with the free nucleons. In spite of these movements, quasi-equilibrium is still a good approximation, with the abundances in the iron peak group, which comprises 80% of the mass by the time  $9.5 \times 10^{-3}$  seconds have passed (corresponding to  $T_9 = 4$  and  $\rho = 5.1 \times 10^8 \text{ g cm}^{-3}$ ), having a spread of a few % from quasi-equilibrium, while those in the silicon group (comprising 10% of the mass) have a spread of roughly 15%.

Figure 2c follows the QSE group evolution further, showing the QSE group structure at

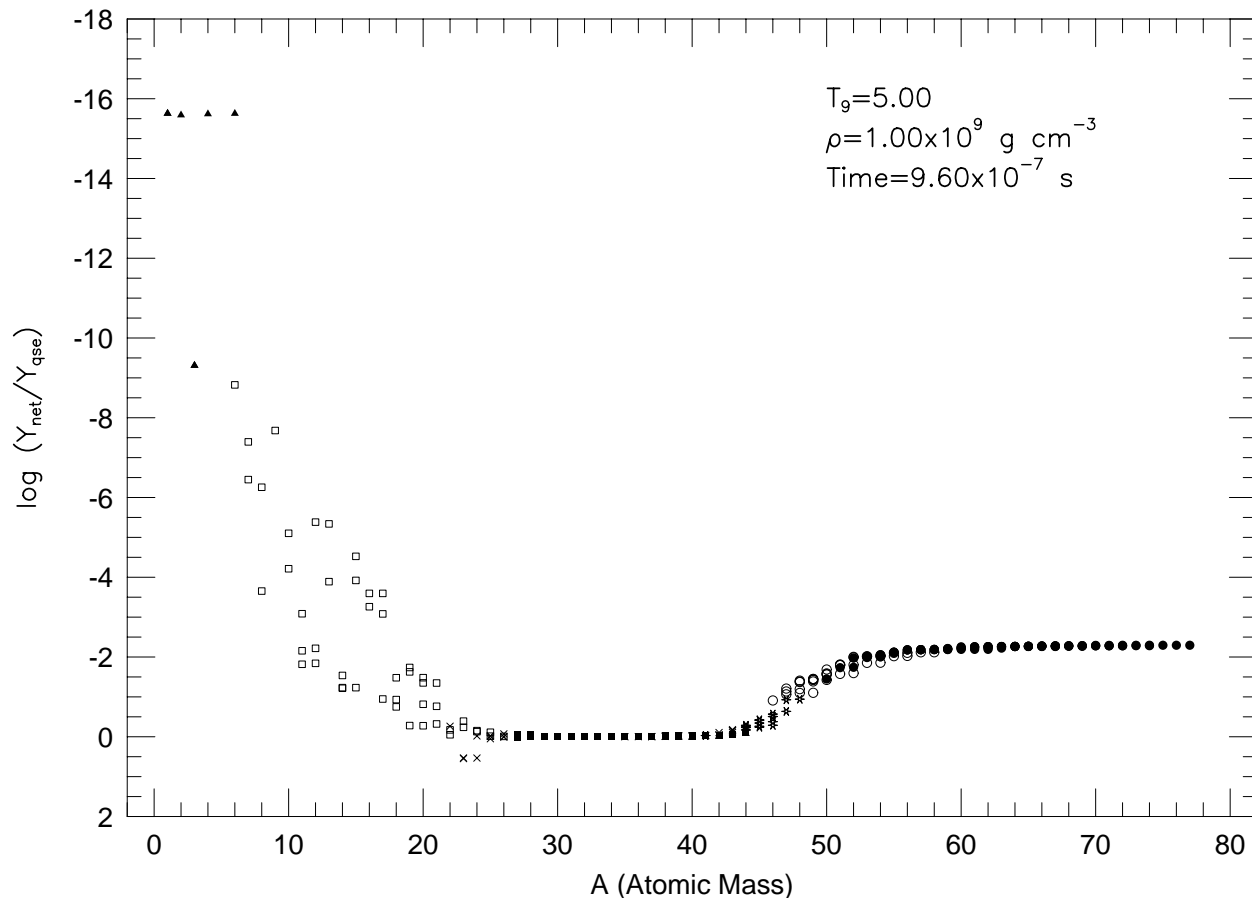


Fig. 2.— (a) Examination of the QSE group structure for  $T_{9i} = 5$ ,  $\rho_i = 10^9 \text{ g cm}^{-3}$ , and  $Y_e = .48$  after elapsed time of  $9.6 \times 10^{-7}$  seconds.  $Y_{net}$  are the network abundances, while  $Y_{qse}$  are abundances calculated assuming QSE from the network abundances of n, p,  $^{28}\text{Si}$ .

an elapsed time of  $1.5 \times 10^{-2}$  seconds, corresponding to  $T_9 = 3.5$  and  $\rho = 3.5 \times 10^8 \text{ g cm}^{-3}$ . As the temperature continues to decline, the trend begun near  $T_9 = 4$  continues, with the light and iron peak QSE groups moving still further from quasi-equilibrium with the silicon group. For  $T_9 = 3.5$ , the spread from quasi-equilibrium among the group abundances is comparable to those for  $T_9 = 4.5$  and 4. Columns 2 and 3 of Table 1 compare the network abundances with those predicted by membership in the appropriate QSE group. The QSE abundances,  $Y_{qse}$ , in all three Tables in this article are calculated from the network abundances of free protons and neutrons and either  $^{28}\text{Si}$  or  $^{56}\text{Ni}$ . Typically the discrepancy is a few %, though somewhat larger at the edges of the groups. By  $T_9 = 3.25$ , quasi-equilibrium is beginning to fail. As a result the silicon and iron peak QSE groups are getting more ragged, with the abundances of the important nuclei within the silicon group having a 25% spread from quasi-equilibrium and the spread within the iron peak group having grown to 10% (ignoring nuclei with abundances smaller than  $10^{-12}$ ). As temperature

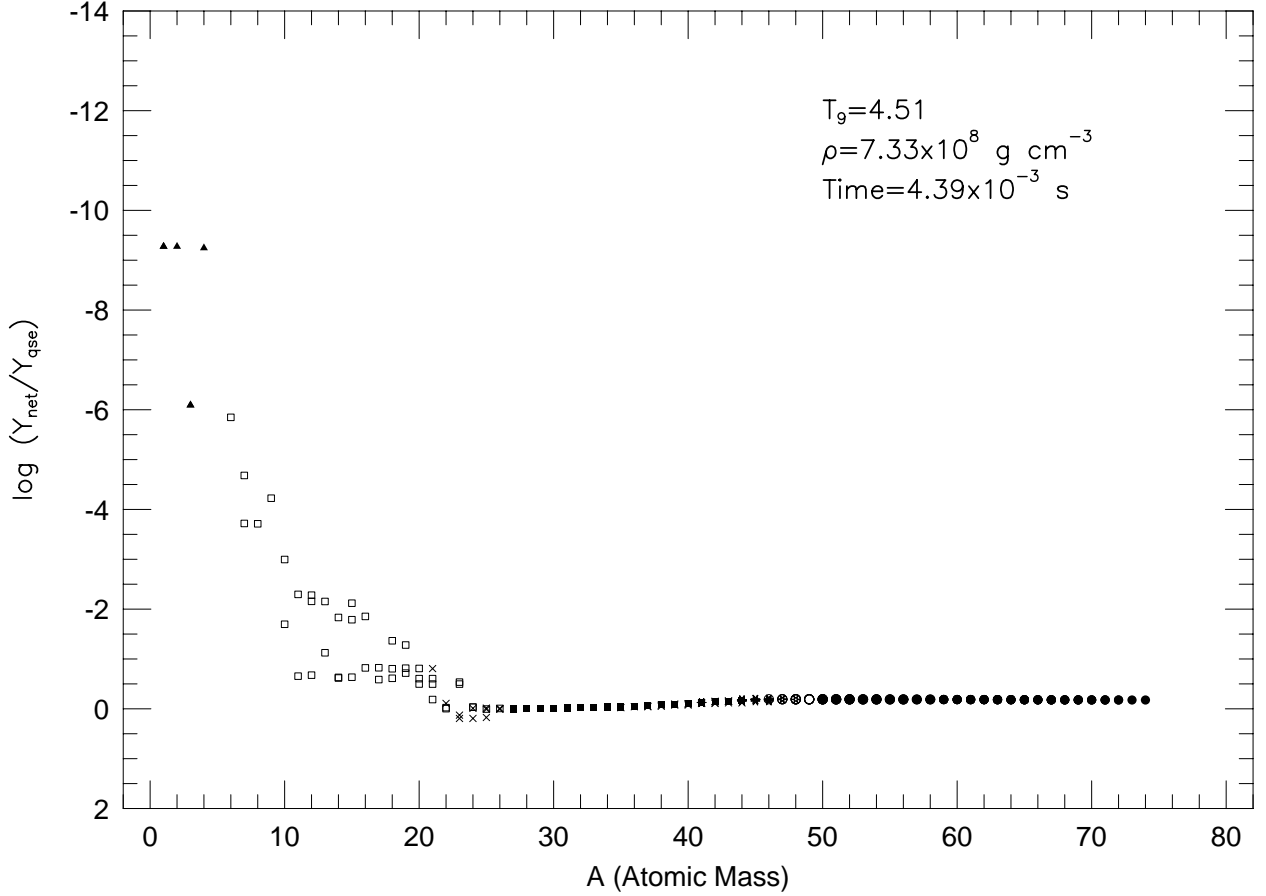


Fig. 2.— (b) Examination of the QSE group structure for  $T_{9i} = 5$ ,  $\rho_i = 10^9 \text{ g cm}^{-3}$ , and  $Y_e = .48$  after elapsed time of  $4.4 \times 10^{-3}$  ( $T_9 = 4.5$ ,  $\rho = 7.3 \times 10^8 \text{ g cm}^{-3}$ ).  $Y_{net}$  are the network abundances, while  $Y_{qse}$  are abundances calculated assuming QSE from the network abundances of n, p,  $^{28}\text{Si}$ .

and density continue to drop, more and more of the photodisintegration reactions which cause quasi-equilibrium freeze out, resulting in declining abundances of the free nucleons and  $\alpha$ -particles. By the time  $T_9 = 3.0$  (elapsed time= $2.2 \times 10^{-2}$  seconds), the abundances of the light nuclei have dropped by more than an order of magnitude, severely skewing the QSE abundance pattern, which is shown in Figure 2d. The silicon QSE group (which still comprises 10% of the mass) displays a shear of almost an order of magnitude between  $^{28}\text{Si}$  and neutron-rich Ar. As comparison of the 4th and 5th columns of Table 1 reveals, important nuclei like  $^{34}\text{S}$  and  $^{36}\text{Ar}$  have abundances less than 50% of that predicted by quasi-equilibrium with  $^{28}\text{Si}$ . Even some of the core nuclei of the iron peak, isotopes of Fe, Co, Ni, Cu and Zn, are displaced by as much as 50% from equilibrium with  $^{56}\text{Ni}$ . Most indicative of the breakdown of quasi-equilibrium, the abundance of  $^4\text{He}$  is 30% smaller than equilibrium with the free nucleons would require. Globally, the breakdown in QSE



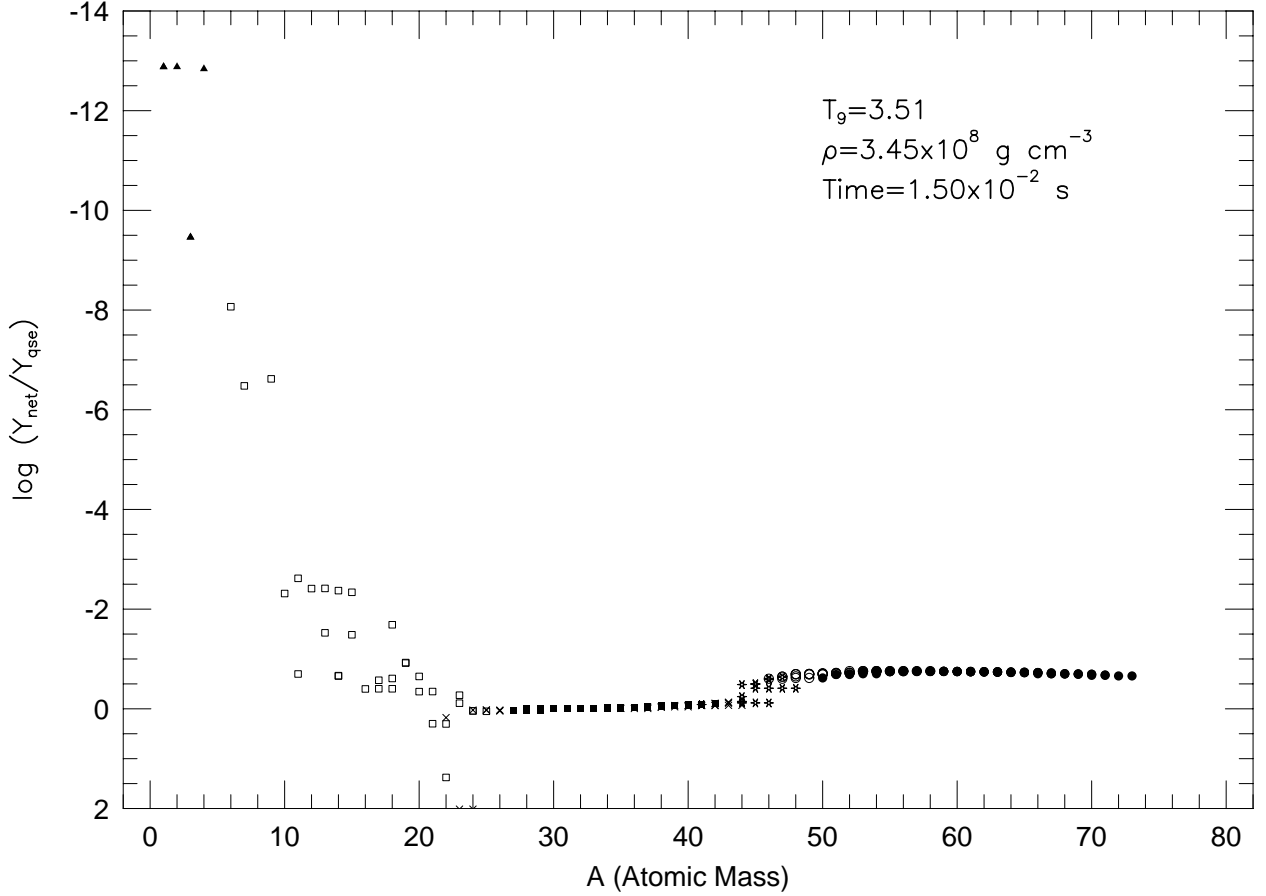


Fig. 2.— (c) Examination of the QSE group structure for  $T_{9i} = 5$ ,  $\rho_i = 10^9 \text{ g cm}^{-3}$ , and  $Y_e = .48$  after elapsed time of  $1.5 \times 10^{-2}$  seconds ( $T_9 = 3.5$ ,  $\rho = 3.5 \times 10^8 \text{ g cm}^{-3}$ ).  $Y_{net}$  are the network abundances, while  $Y_{qse}$  are abundances calculated assuming QSE from the network abundances of n, p,  $^{28}\text{Si}$ .

also implies that the QSE abundances no longer satisfy the nucleon number conservation relation,  $\sum AY$ . While network convergence conditions require that  $\sum AY_{net}$  change by less than one part in  $10^6$  during a timestep,  $\sum AY_{qse} \sim 1.3$  at this point.

Further decline in temperature and density results in further reductions in the light nuclear abundances. As comparison of columns 4 and 7 of Table 1 reveals, between  $2.2 \times 10^{-2}$  and  $4.2 \times 10^{-2}$  seconds, corresponding to  $T_9 = 3.0$  and  $T_9 = 1.85$ , the abundances of the free protons and  $\alpha$ -particles drop by roughly five more orders of magnitude, with the free neutron abundance dropping by more than 8 more order of magnitude. While these continued captures remove any hint of quasi-equilibrium with the current free nucleon abundances, further examination of columns 4 and 7 of Table 1 reveals that the most important products (those with mass fractions greater than .1%) have undergone only small changes in abundance. Even though quasi-equilibrium has become suspect by  $T_9 = 3.0$ ,

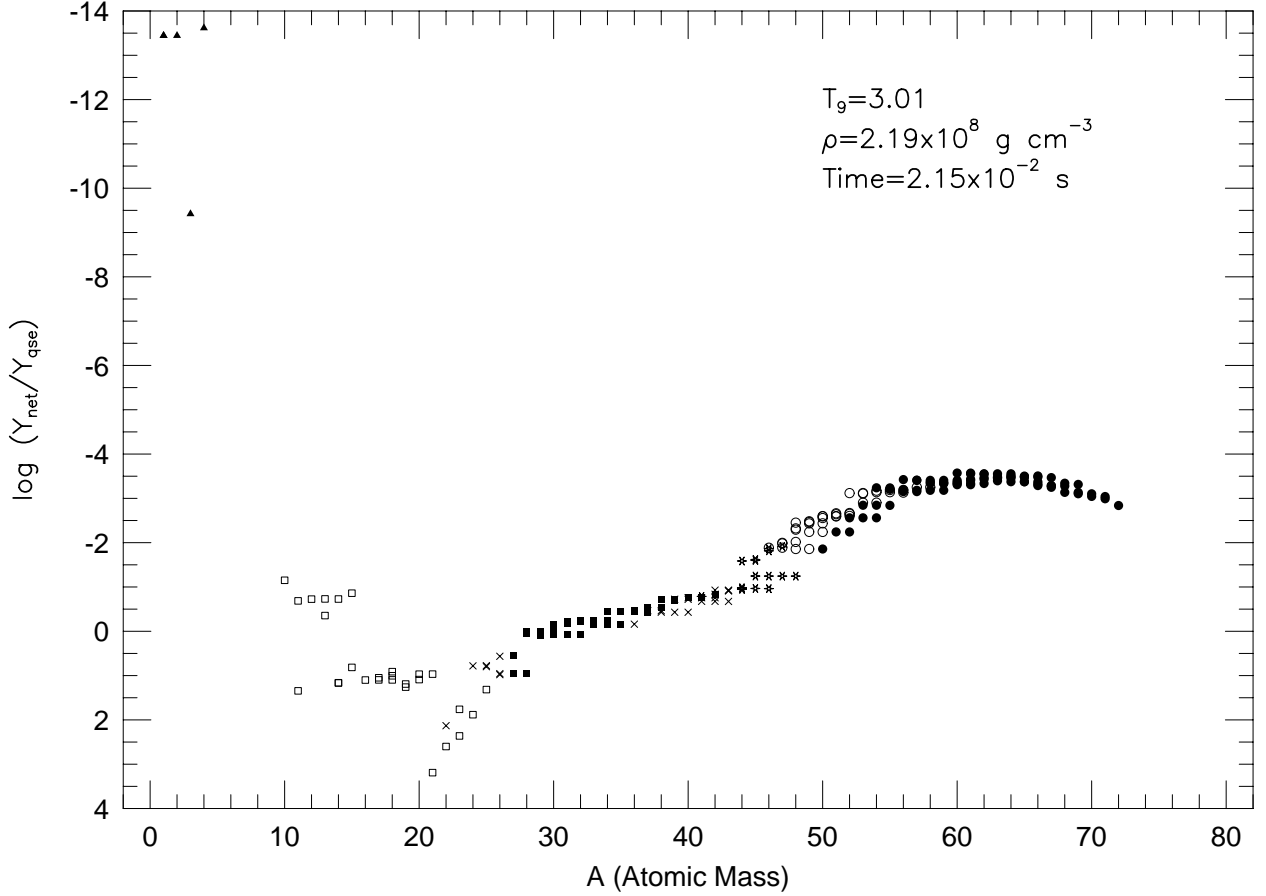


Fig. 2.— (d) Examination of the QSE group structure for  $T_{9i} = 5$ ,  $\rho_i = 10^9 \text{ g cm}^{-3}$ , and  $Y_e = .48$  after elapsed time of  $2.2 \times 10^{-2}$  seconds ( $T_9 = 3.0$ ,  $\rho = 2.2 \times 10^8 \text{ g cm}^{-3}$ ).  $Y_{net}$  are the network abundances, while  $Y_{qse}$  are abundances calculated assuming QSE from the network abundances of n, p,  $^{28}\text{Si}$ .

abundances calculated assuming QSE (using the network values of the abundances of  $^{28}\text{Si}$ ,  $^{56}\text{Ni}$ , free protons and neutrons), at this temperature (column 5 of Table 1) are a better estimate of the final abundances than those predicted by the freezeout of NSE at  $T_9 = 3.0$  (shown in column 6 of Table 1). While this is not surprising for a case which fails to exhaust silicon, it is still worth noting that the relative abundances among the dominant iron peak nuclei are also better predicted by QSE than NSE. As we discussed in HT96, QSE and the greater binding energy of the neutron rich members of the iron peak group result in preferential storage of neutrons in the iron peak group. In this case, even though the iron peak group contains 90% of the mass fraction, comparison of the network abundances at  $T_9=3$  (column 5) to the corresponding NSE abundances (column 7) reveals significant enhancement of the neutron-rich iron peak nuclei. Such enhancements are better estimated by QSE than NSE. For example, the ratio of the QSE abundances of  $^{56}\text{Fe}$  to  $^{54}\text{Fe}$  frozen at

Table 1: Selected abundances near freezeout for the *incomplete burning* example ( $T_{9i} = 5$ ,  $\rho_i = 10^9 \text{ g cm}^{-3}$  and  $Y_e = .48$ )

Time (s)	$1.50 \times 10^{-2}$		$2.15 \times 10^{-2}$			$4.21 \times 10^{-2}$
$T_9$	3.51		3.01			1.85
$\rho$ ( $\text{g cm}^{-3}$ )	$3.45 \times 10^8$		$2.18 \times 10^8$			$5.05 \times 10^7$
Nucleus	$Y_{net}$	$Y_{qse}$	$Y_{net}$	$Y_{qse}$	$Y_{nse}$	$Y_{net}$
n	$2.67 \times 10^{-13}$	$2.67 \times 10^{-13}$	$1.66 \times 10^{-15}$	$1.66 \times 10^{-15}$	$1.06 \times 10^{-15}$	$8.68 \times 10^{-24}$
p	$8.49 \times 10^{-9}$	$8.49 \times 10^{-9}$	$1.93 \times 10^{-10}$	$1.93 \times 10^{-10}$	$7.59 \times 10^{-10}$	$4.76 \times 10^{-16}$
$^4\text{He}$	$2.08 \times 10^{-8}$	$1.90 \times 10^{-8}$	$6.44 \times 10^{-10}$	$9.56 \times 10^{-10}$	$6.11 \times 10^{-9}$	$1.26 \times 10^{-14}$
$^{28}\text{Si}$	$2.50 \times 10^{-3}$	$2.50 \times 10^{-3}$	$2.49 \times 10^{-3}$	$2.49 \times 10^{-3}$	$4.08 \times 10^{-11}$	$2.49 \times 10^{-3}$
$^{30}\text{Si}$	$3.69 \times 10^{-6}$	$3.75 \times 10^{-6}$	$2.12 \times 10^{-6}$	$3.04 \times 10^{-6}$	$2.04 \times 10^{-14}$	$1.72 \times 10^{-6}$
$^{32}\text{S}$	$8.03 \times 10^{-4}$	$8.21 \times 10^{-4}$	$8.24 \times 10^{-4}$	$1.45 \times 10^{-3}$	$1.54 \times 10^{-10}$	$8.27 \times 10^{-4}$
$^{34}\text{S}$	$2.87 \times 10^{-5}$	$3.10 \times 10^{-5}$	$2.76 \times 10^{-5}$	$7.58 \times 10^{-5}$	$3.30 \times 10^{-12}$	$2.66 \times 10^{-5}$
$^{36}\text{Ar}$	$1.00 \times 10^{-4}$	$1.07 \times 10^{-4}$	$9.67 \times 10^{-5}$	$2.83 \times 10^{-4}$	$1.95 \times 10^{-10}$	$9.74 \times 10^{-5}$
$^{38}\text{Ar}$	$2.22 \times 10^{-5}$	$2.59 \times 10^{-5}$	$2.43 \times 10^{-5}$	$1.29 \times 10^{-4}$	$3.66 \times 10^{-11}$	$2.42 \times 10^{-5}$
$^{40}\text{Ca}$	$4.83 \times 10^{-5}$	$5.62 \times 10^{-5}$	$4.88 \times 10^{-5}$	$2.79 \times 10^{-4}$	$1.25 \times 10^{-9}$	$4.92 \times 10^{-5}$
$^{42}\text{Ca}$	$8.22 \times 10^{-7}$	$1.06 \times 10^{-6}$	$7.51 \times 10^{-7}$	$6.35 \times 10^{-6}$	$1.17 \times 10^{-11}$	$7.50 \times 10^{-7}$
$^{46}\text{Ti}$	$4.56 \times 10^{-6}$	$3.22 \times 10^{-6}$	$4.12 \times 10^{-6}$	$2.24 \times 10^{-7}$	$3.83 \times 10^{-9}$	$4.13 \times 10^{-6}$
$^{48}\text{Ti}$	$5.55 \times 10^{-7}$	$4.86 \times 10^{-7}$	$3.05 \times 10^{-7}$	$6.09 \times 10^{-8}$	$4.27 \times 10^{-10}$	$2.78 \times 10^{-7}$
$^{54}\text{Fe}$	$1.09 \times 10^{-2}$	$1.09 \times 10^{-2}$	$1.13 \times 10^{-2}$	$1.38 \times 10^{-2}$	$9.59 \times 10^{-3}$	$1.13 \times 10^{-2}$
$^{56}\text{Fe}$	$2.12 \times 10^{-3}$	$2.13 \times 10^{-3}$	$2.35 \times 10^{-3}$	$4.39 \times 10^{-3}$	$1.26 \times 10^{-3}$	$2.37 \times 10^{-3}$
$^{58}\text{Fe}$	$3.23 \times 10^{-8}$	$3.21 \times 10^{-8}$	$1.61 \times 10^{-8}$	$2.47 \times 10^{-8}$	$2.90 \times 10^{-9}$	$1.50 \times 10^{-8}$
$^{56}\text{Ni}$	$7.02 \times 10^{-6}$	$7.02 \times 10^{-6}$	$2.33 \times 10^{-6}$	$2.33 \times 10^{-6}$	$2.53 \times 10^{-5}$	$2.06 \times 10^{-6}$
$^{58}\text{Ni}$	$7.67 \times 10^{-4}$	$7.65 \times 10^{-4}$	$7.12 \times 10^{-4}$	$1.28 \times 10^{-3}$	$5.69 \times 10^{-3}$	$7.14 \times 10^{-4}$
$^{60}\text{Ni}$	$8.67 \times 10^{-5}$	$8.45 \times 10^{-5}$	$8.74 \times 10^{-5}$	$2.29 \times 10^{-4}$	$4.18 \times 10^{-4}$	$8.75 \times 10^{-5}$
$^{60}\text{Zn}$	$3.10 \times 10^{-12}$	$3.09 \times 10^{-12}$	$9.40 \times 10^{-14}$	$1.68 \times 10^{-13}$	$1.16 \times 10^{-11}$	$2.48 \times 10^{-15}$
$^{62}\text{Zn}$	$3.09 \times 10^{-9}$	$3.00 \times 10^{-9}$	$4.66 \times 10^{-10}$	$1.18 \times 10^{-9}$	$3.34 \times 10^{-8}$	$2.49 \times 10^{-10}$
$^{64}\text{Zn}$	$2.32 \times 10^{-9}$	$2.18 \times 10^{-9}$	$8.78 \times 10^{-10}$	$1.97 \times 10^{-9}$	$2.30 \times 10^{-8}$	$8.27 \times 10^{-10}$

$T_9=3.5$  is .20. This is much closer to the final network ratio  $Y(^{56}\text{Fe})/Y(^{54}\text{Fe}) = .21$  than that predicted by NSE frozen around  $T_9=3$  (.14).

If our hope to in the future use QSE to reduce the computational cost of silicon burning nucleosynthesis is to be realized, we must understand where we can safely employ QSE. Clearly, the sharp drop in the free nucleon abundances, and the attendant departure from QSE, seen in this case below  $T_9=3.0$ , can not be followed by a method employing QSE. However, since abundances other than the free nucleons and  $\alpha$ -particles are little affected, we can provide reasonable estimates for the final abundances by freezing the QSE abundances prior to the actual freezeout of photodisintegrations. For example, comparison of columns 3 and 7 of Table 1, reveals that the QSE abundance, frozen at  $T_9 = 3.5$ , provides

good ( $\pm 10\%$ ) estimates of the final nuclear abundances for all of the abundances larger than  $10^{-5}$ . Thus we conclude that quasi-equilibrium and, by extension, future methods which employ quasi-equilibrium, can provide good abundance estimates for cases of silicon burning which fail to reach silicon exhaustion and that these estimates are significantly better than those based on NSE.

### 3. Normal Freezeout

The next test of the applicability of quasi-equilibrium is that of complete silicon burning and the *normal freezeout*, where previous authors have indicated that the nuclei within the mass zone reach NSE and then remain in NSE as the mass zone cools. To this end, we present an example with  $T_{9i} = 6$ ,  $\rho = 10^9 \text{ g cm}^{-3}$ , and  $Y_e = .48$ . Early in the calculation, after an elapsed time of  $2.0 \times 10^{-8}$  seconds, the QSE group structure shows clear evidence of three distinct groups, with the abundances of the iron peak and light QSE groups being one and ten orders of magnitude smaller, respectively, than equilibrium with the silicon QSE group would require. As in the previous example, these groups initially converge toward mutual equilibrium. By the time  $5.1 \times 10^{-7}$  seconds have passed, with 75% of the mass still concentrated within the original silicon group, the iron peak and silicon groups reach mutual equilibrium.

After an elapsed time of  $1.7 \times 10^{-4}$  seconds, the temperature has dropped to  $T_9 = 5.98$ , with a density of  $9.9 \times 10^8 \text{ g cm}^{-3}$ . As Figure 3a demonstrates, the convergence of the QSE groups has continued, with the abundances of the light group now greater than 1% of their silicon quasi-equilibrium abundance. The combined silicon and iron peak QSE group now stretches as far as  $A=10$ , with the abundances of  $^{12}\text{C}$ ,  $^{16}\text{O}$ , and  $^{20}\text{Ne}$  all being within 25% of quasi-equilibrium with  $^{28}\text{Si}$ . The deviations near  $A=19$  are due to an unbalanced reaction in the reaction rate library. While this error effects  $^{19}\text{F}$  and, to a lesser extent, several of its neighbors with trace abundances, it is unimportant to the dominant flows which link the light QSE group to the silicon QSE group. Though the members of this large QSE group dominate the mass fraction, the absence of the free nucleons from the unified QSE group indicates that NSE is not yet fully established. Figure 4a compares the network abundances at this point in the calculation to the abundances that NSE predicts for these conditions. For Figures 4 and 6, the filled shapes represent network abundances larger than  $10^{-6}$ , and the hollow shapes denote abundances less than  $10^{-12}$ . The sided-ness of the shapes still identifies their QSE group membership as in Figures 2, 3 & 5. By this time ( $1.7 \times 10^{-4}$  s), the dominant members of the iron peak (which now contain almost 90% of the mass) and the light nuclei (which represent roughly 0.3% of the mass) are very close to NSE. However the nuclei from carbon through silicon, though in quasi-equilibrium, lag behind with abundances as much as an order of magnitude larger than NSE would predict.

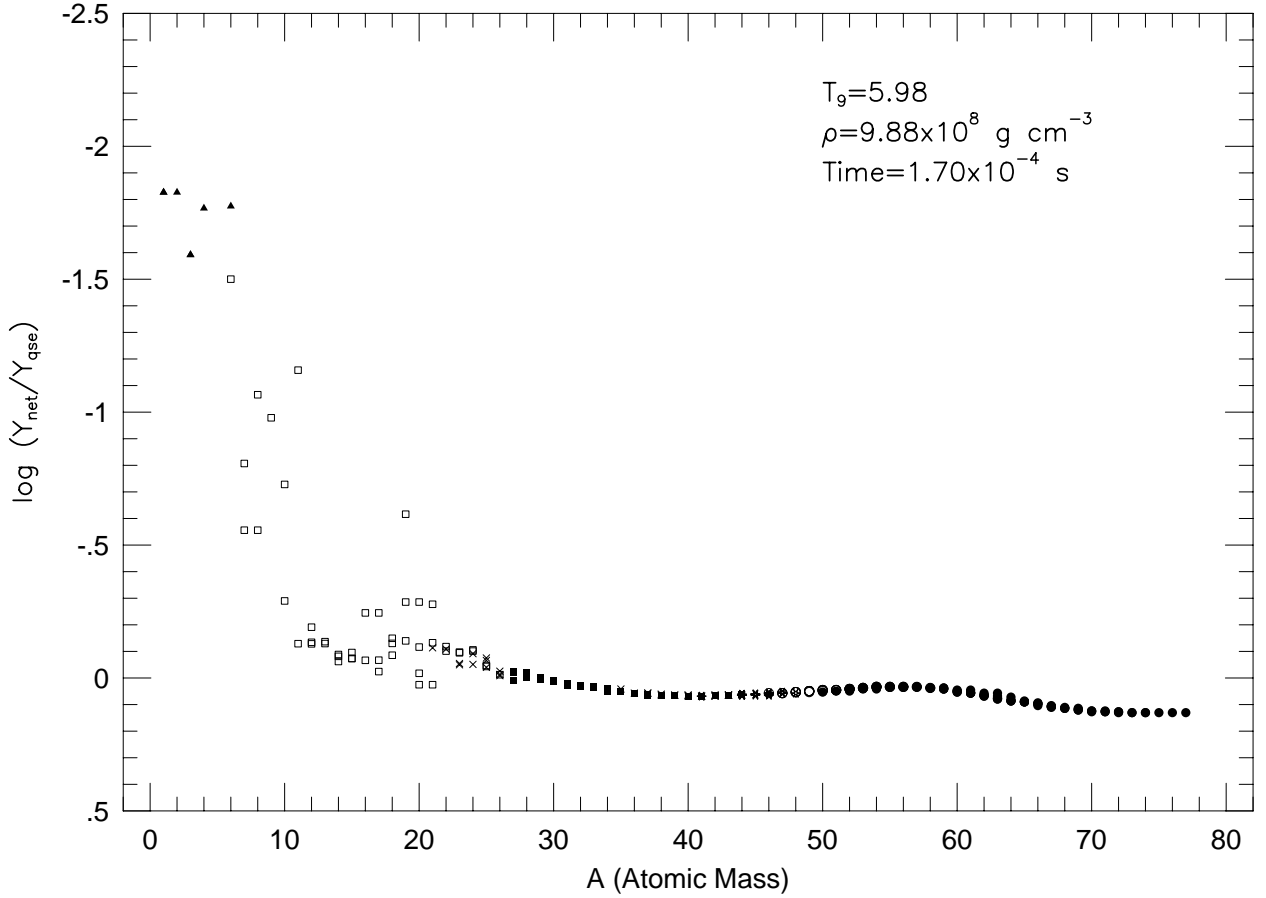


Fig. 3.— (a) Examination of the QSE group structure for  $T_{9i} = 6$ ,  $\rho_i = 10^9 \text{ g cm}^{-3}$ , and  $Y_e = .48$ , after elapsed times of  $1.70 \times 10^{-4}$  seconds ( $T_9 = 5.98$  and  $\rho = 9.88 \times 10^8 \text{ g cm}^{-3}$ ).  $Y_{net}$  are the network abundances, while  $Y_{qse}$  are abundances calculated assuming QSE from the network abundances of n, p,  $^{28}\text{Si}$ .

As the calculation continues, these laggards converge further toward the current NSE abundance pattern. However, significant discrepancies remain between the network abundances and those predicted by NSE for the intermediate mass nuclei. For example, by an elapsed time of  $1.5 \times 10^{-3}$  seconds ( $T_9 = 5.8$  and  $\rho = 9.0 \times 10^8 \text{ g cm}^{-3}$ ),  $^{28}\text{Si}$  is nearly 3 times more abundant than it would be if NSE were completely established. Quasi-equilibrium provides a better estimate for many nuclei, with the single QSE group stretching from carbon to germanium displaying deviations from quasi-equilibrium of less than 25%. As our hypothetical hydrodynamic mass zone continues to expand and cool, the abundance distribution never catches up with NSE. By an elapsed time of  $1.7 \times 10^{-2}$  seconds, with  $T_9$  having dropped to 4.0 and  $\rho$  to  $3.0 \times 10^8 \text{ g cm}^{-3}$ , the network abundances for the intermediate mass elements are not significantly closer to those calculated from NSE, with  $^{28}\text{Si}$  remaining 2.5 times more abundant than predicted by NSE. The single

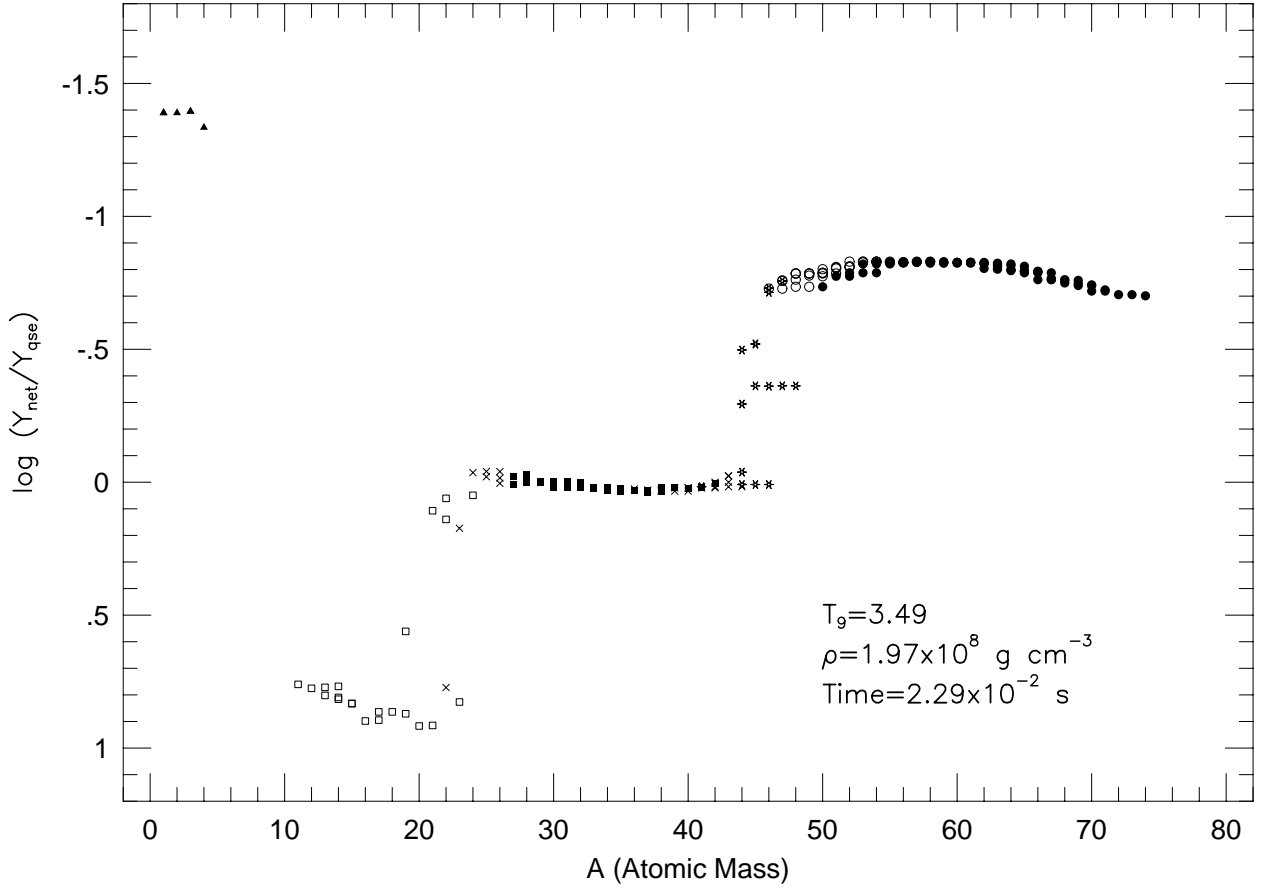


Fig. 3.— (b) Examination of the QSE group structure for  $T_{9i} = 6$ ,  $\rho_i = 10^9 \text{ g cm}^{-3}$ , and  $Y_e = .48$ , after elapsed time of  $2.29 \times 10^{-2}$  seconds ( $T_9 = 3.49$  and  $\rho = 1.97 \times 10^8 \text{ g cm}^{-3}$ ).  $Y_{net}$  are the network abundances, while  $Y_{qse}$  are abundances calculated assuming QSE from the network abundances of n, p,  $^{28}\text{Si}$ .

large QSE group has also begun to fragment. By the time the temperature has dropped to  $T_9 = 3.5$  (elapsed time =  $2.29 \times 10^{-2}$  seconds), there are 4 distinct QSE groups. As Figure 3b shows, the silicon and iron groups are again distinct, separated by a fringe of nuclei;  $^{45}\text{K}$ ,  $^{44}\text{Ca}$ ,  $^{45}\text{Ca}$ ,  $^{45}\text{Sc}$ ,  $^{45}\text{Ti}$ ,  $^{46}\text{V}$ ,  $^{47}\text{Cr}$ , and  $^{48}\text{Mn}$ . These nuclei are familiar from the analysis presented in HT96. As the QSE groups separate, the fracture occurs where they were joined. Comparison of columns 2 and 3 of Table 2 reveals that within these groups, the abundances predicted by QSE differ by only a few % from the network abundances. In addition to these groups and the light group, the nuclei in the C-O-Ne region are within 25% of mutual equilibrium. These nuclei are almost an order of magnitude overabundant for quasi-equilibrium with the silicon group. Comparison between the network abundances and those predicted by NSE, shown in Figure 4b, reveals larger discrepancies, with the C-O-Ne nuclei roughly 2 orders of magnitude more abundant than NSE would predict and

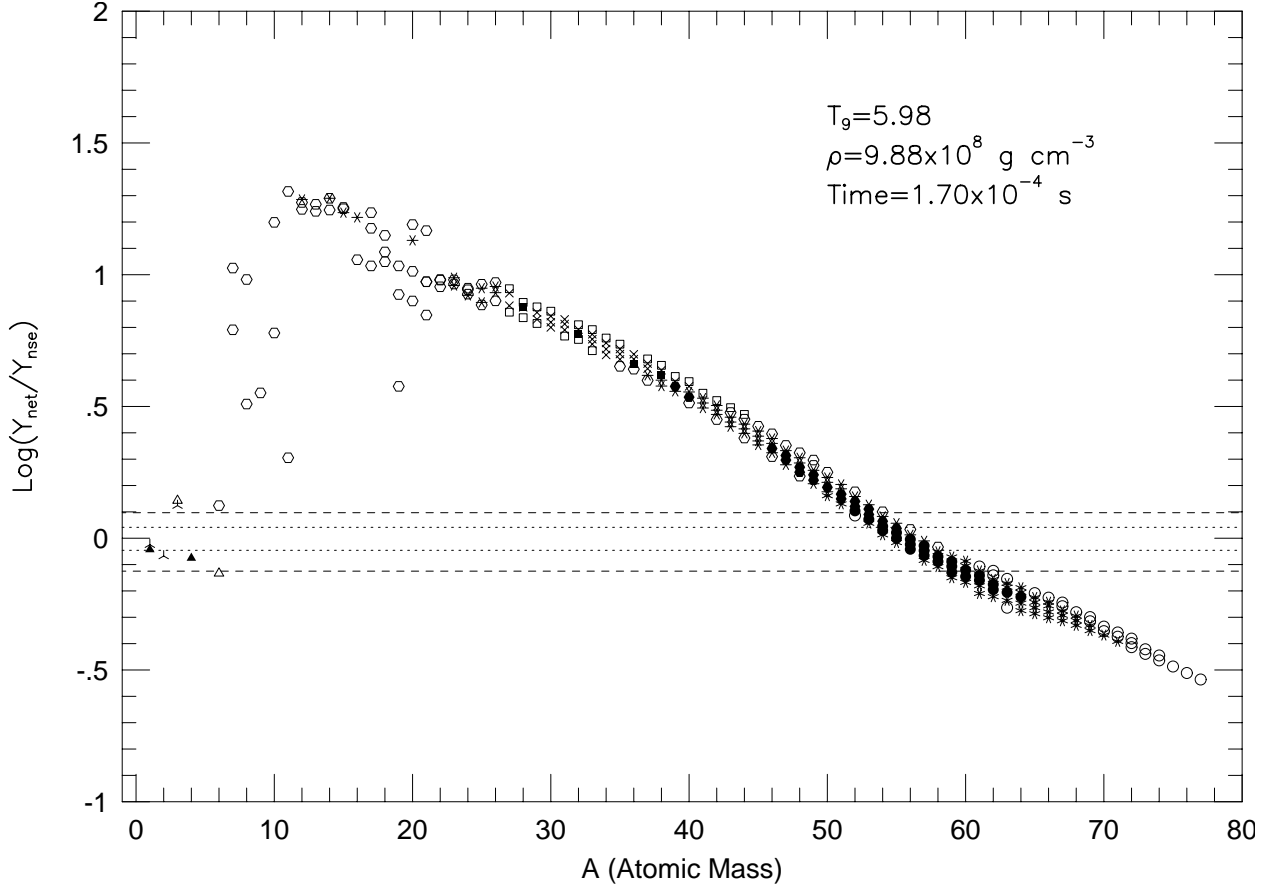


Fig. 4.— (a) Comparison of the network abundances to the NSE abundances for a case with  $T_{9i} = 6$ ,  $\rho_i = 10^9 \text{ g cm}^{-3}$ , and  $Y_e = .48$ , after elapsed times of  $1.7 \times 10^{-4}$  seconds ( $T_9 = 5.98$  and  $\rho = 9.9 \times 10^8 \text{ g cm}^{-3}$ ). The filled shapes represent network abundances larger than  $10^{-6}$ , and the hollow shapes denote abundances less than  $10^{-12}$ .

the silicon group an order of magnitude overabundant. The abundances within the light group and the iron peak group, which, now contains more than 99% of the mass, are quite close to their NSE values.

In this case, like that discussed in the previous section, in the vicinity of  $T_9 = 3.0$ , quasi-equilibrium breaks down. Though the discrepancies between the network and QSE abundances (which are based on the network abundances of n, p,  $^{28}\text{Si}$  and  $^{56}\text{Ni}$ ) at  $T_9 = 3.5$  (columns 2 and 3 of Table 2) are small, examination of columns 4 and 5 of Table 2 reveals much larger differences by the time  $T_9 = 3.0$ . Among the nuclei which dominate the mass fraction, slightly neutron rich members of the iron group, predictions based on QSE err by as much as 50%. It is the decline in the abundances of the light nuclei, which drop by more than an order of magnitude between  $T_9 = 3.5$  and  $T_9 = 3.0$ , which cause this discrepancy.

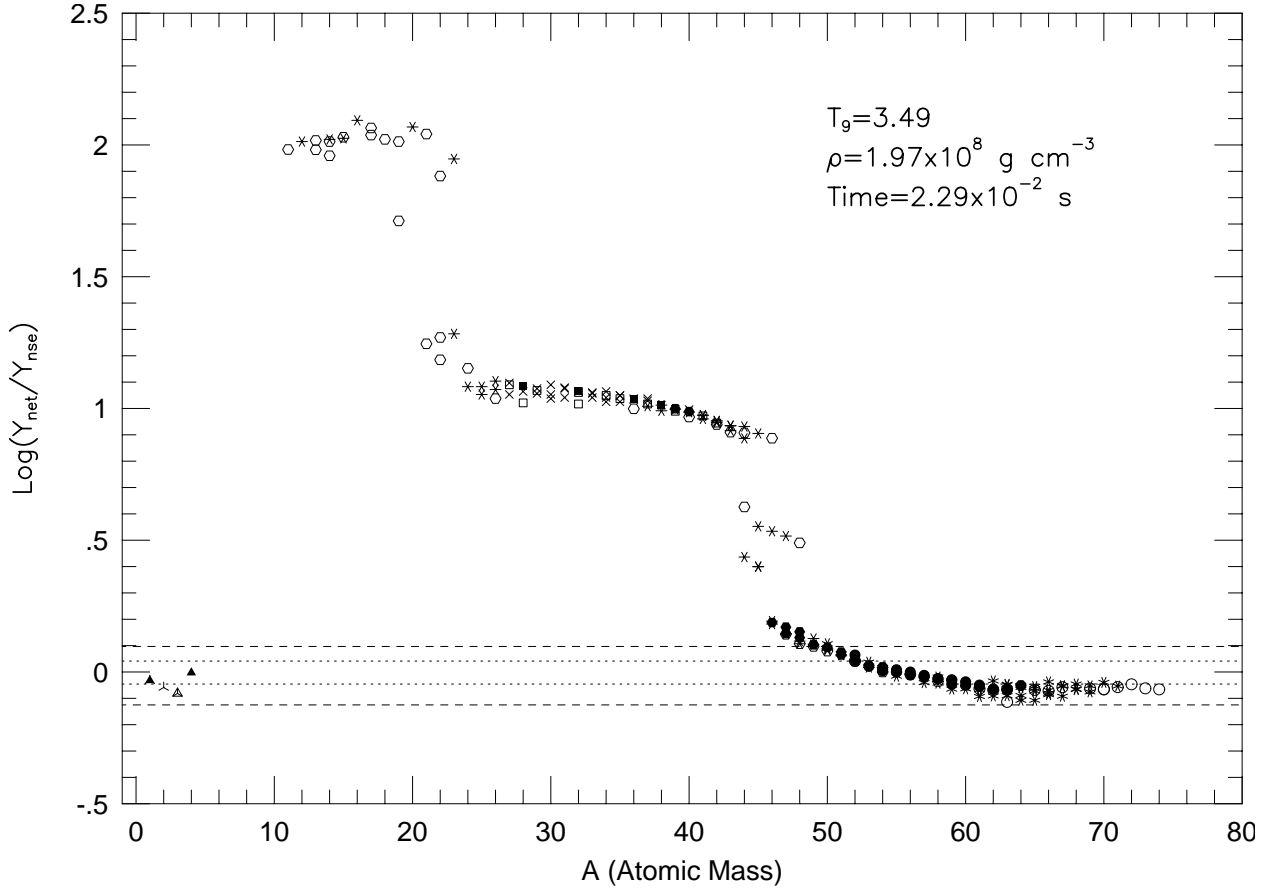


Fig. 4.— (b) Comparison of the network abundances to the NSE abundances for a case with  $T_{9i} = 6$ ,  $\rho_i = 10^9 \text{ g cm}^{-3}$ , and  $Y_e = .48$ , after elapsed time of  $2.3 \times 10^{-2}$  seconds ( $T_9 = 3.5$  and  $\rho = 1.97 \times 10^8 \text{ g cm}^{-3}$ ). The filled shapes represent network abundances larger than  $10^{-6}$ , and the hollow shapes denote abundances less than  $10^{-12}$ .

Comparison of the abundances of the dominant members of the iron peak group with abundance predictions based on NSE (column 6 of Table 2), confirms that NSE does provide a good estimate of the iron group (and light group) abundances. However the differences between the network and NSE for intermediate nuclei persist. For example,  $^{40}\text{Ca}$ , the most abundant of the intermediate mass elements with a mass fraction of  $9 \times 10^{-6}$ , is 160 times more abundant than NSE would predict at  $T_9=3.0$ . As Column 7 of Table 2 reveals, these over abundances of the intermediate mass elements persist once the final freezeout occurs. This is consistent with the results of Meyer, Krishnan, & Clayton (1996), who found that, for significantly more neutronized material, such high density (low entropy) cases can result in final abundances of  $^{48}\text{Ca}$  as large as .01, millions of times what NSE, frozen at  $T_9=3.5$ , would predict. Comparison of columns 7 and 4 also reveals that in this case, like the previous, the abundances of the light group nuclei are the only ones which change markedly



Table 2: Selected abundances near freezeout for the *normal freezeout* example ( $T_{9i} = 6$ ,  $\rho_i = 10^9 \text{ g cm}^{-3}$  and  $Y_e = .48$ )

Time (s)	$2.29 \times 10^{-2}$		$2.93 \times 10^{-2}$			$5.10 \times 10^{-2}$
$T_9$	3.49		3.00			1.80
$\rho$ ( $\text{g cm}^{-3}$ )	$1.97 \times 10^8$		$1.25 \times 10^8$			$2.68 \times 10^7$
Nucleus	$Y_{net}$	$Y_{qse}$	$Y_{net}$	$Y_{qse}$	$Y_{nse}$	$Y_{net}$
n	$3.26 \times 10^{-13}$	$3.26 \times 10^{-13}$	$1.96 \times 10^{-15}$	$1.96 \times 10^{-15}$	$1.68 \times 10^{-15}$	$3.74 \times 10^{-24}$
p	$5.01 \times 10^{-8}$	$5.01 \times 10^{-8}$	$1.35 \times 10^{-9}$	$1.35 \times 10^{-9}$	$1.30 \times 10^{-9}$	$2.65 \times 10^{-15}$
$^4\text{He}$	$2.93 \times 10^{-7}$	$2.58 \times 10^{-7}$	$1.34 \times 10^{-8}$	$1.57 \times 10^{-8}$	$1.07 \times 10^{-8}$	$3.10 \times 10^{-10}$
$^{28}\text{Si}$	$2.42 \times 10^{-8}$	$2.42 \times 10^{-8}$	$1.82 \times 10^{-8}$	$1.82 \times 10^{-8}$	$6.35 \times 10^{-11}$	$1.76 \times 10^{-8}$
$^{30}\text{Si}$	$2.34 \times 10^{-11}$	$2.23 \times 10^{-11}$	$9.70 \times 10^{-12}$	$1.20 \times 10^{-11}$	$3.10 \times 10^{-14}$	$6.47 \times 10^{-12}$
$^{32}\text{S}$	$6.03 \times 10^{-8}$	$5.76 \times 10^{-8}$	$5.55 \times 10^{-8}$	$9.15 \times 10^{-8}$	$2.18 \times 10^{-10}$	$5.55 \times 10^{-8}$
$^{34}\text{S}$	$1.45 \times 10^{-9}$	$1.35 \times 10^{-9}$	$1.14 \times 10^{-9}$	$2.61 \times 10^{-9}$	$4.59 \times 10^{-12}$	$9.64 \times 10^{-10}$
$^{36}\text{Ar}$	$5.71 \times 10^{-8}$	$5.34 \times 10^{-8}$	$5.58 \times 10^{-8}$	$1.50 \times 10^{-7}$	$2.43 \times 10^{-10}$	$5.64 \times 10^{-8}$
$^{38}\text{Ar}$	$8.43 \times 10^{-9}$	$8.04 \times 10^{-9}$	$7.52 \times 10^{-9}$	$3.77 \times 10^{-8}$	$4.52 \times 10^{-11}$	$6.67 \times 10^{-9}$
$^{40}\text{Ca}$	$2.04 \times 10^{-7}$	$1.95 \times 10^{-7}$	$2.18 \times 10^{-7}$	$1.22 \times 10^{-6}$	$1.36 \times 10^{-9}$	$2.20 \times 10^{-7}$
$^{42}\text{Ca}$	$2.29 \times 10^{-9}$	$2.29 \times 10^{-9}$	$2.12 \times 10^{-9}$	$1.52 \times 10^{-8}$	$1.25 \times 10^{-11}$	$2.13 \times 10^{-9}$
$^{46}\text{Ti}$	$5.08 \times 10^{-8}$	$4.05 \times 10^{-8}$	$3.59 \times 10^{-8}$	$1.95 \times 10^{-9}$	$3.49 \times 10^{-9}$	$3.62 \times 10^{-8}$
$^{48}\text{Ti}$	$4.21 \times 10^{-9}$	$3.82 \times 10^{-9}$	$1.33 \times 10^{-9}$	$2.92 \times 10^{-10}$	$3.85 \times 10^{-10}$	$9.04 \times 10^{-10}$
$^{54}\text{Fe}$	$9.53 \times 10^{-3}$	$9.58 \times 10^{-3}$	$9.88 \times 10^{-3}$	$1.17 \times 10^{-2}$	$9.73 \times 10^{-3}$	$9.93 \times 10^{-3}$
$^{56}\text{Fe}$	$1.15 \times 10^{-3}$	$1.16 \times 10^{-3}$	$1.22 \times 10^{-3}$	$2.04 \times 10^{-3}$	$1.26 \times 10^{-3}$	$1.22 \times 10^{-3}$
$^{58}\text{Fe}$	$1.05 \times 10^{-8}$	$1.06 \times 10^{-8}$	$3.84 \times 10^{-9}$	$6.17 \times 10^{-9}$	$2.80 \times 10^{-9}$	$2.99 \times 10^{-9}$
$^{56}\text{Ni}$	$7.29 \times 10^{-5}$	$7.29 \times 10^{-5}$	$3.19 \times 10^{-5}$	$3.19 \times 10^{-5}$	$2.46 \times 10^{-5}$	$2.90 \times 10^{-5}$
$^{58}\text{Ni}$	$5.04 \times 10^{-3}$	$5.07 \times 10^{-3}$	$5.30 \times 10^{-3}$	$9.77 \times 10^{-3}$	$5.56 \times 10^{-3}$	$5.34 \times 10^{-3}$
$^{60}\text{Ni}$	$3.49 \times 10^{-4}$	$3.49 \times 10^{-4}$	$3.57 \times 10^{-4}$	$9.61 \times 10^{-4}$	$4.04 \times 10^{-4}$	$3.58 \times 10^{-4}$
$^{60}\text{Zn}$	$2.10 \times 10^{-10}$	$2.11 \times 10^{-10}$	$9.96 \times 10^{-12}$	$1.82 \times 10^{-11}$	$9.59 \times 10^{-12}$	$4.48 \times 10^{-13}$
$^{62}\text{Zn}$	$1.33 \times 10^{-7}$	$1.32 \times 10^{-7}$	$2.84 \times 10^{-8}$	$7.16 \times 10^{-8}$	$2.78 \times 10^{-8}$	$1.72 \times 10^{-8}$
$^{64}\text{Zn}$	$6.47 \times 10^{-8}$	$6.02 \times 10^{-8}$	$3.01 \times 10^{-8}$	$6.63 \times 10^{-8}$	$1.90 \times 10^{-8}$	$2.89 \times 10^{-8}$

between  $T_9= 3.0$  and  $T_9=1.8$ .

As in the previous example, comparison of the network abundances at freezeout with those corresponding to  $T_9=3.5$  reveals relatively little change. As a result, abundances predicted assuming QSE but frozen around  $T_9=3.5$  provide a good estimate for the final abundances of all nuclei save the lightest. As comparison of columns 3 and 7 of Table 2 reveals, for the most abundant species (those with mass fractions greater than .002) and many other species, this estimate is within 5% of the final abundance. Among the iron peak nuclei which dominate the mass fraction, these abundance predictions are comparable to those based on NSE while among the intermediate mass elements they are better by more than an order of magnitude. As we discussed earlier, once the principal nucleus of a

QSE group reaches equilibrium with the free nucleons, the equations of quasi-equilibrium are identical to those of NSE. Thus it is not surprising that quasi-equilibrium can provide estimates of abundances that agree well with NSE. However, with this example we have demonstrated that quasi-equilibrium can provide a better estimate of the abundances of individual species than NSE when the network is chasing the receding target of complete equilibrium. Thus analysis of this example and others which result in normal freezeout indicate the quasi-equilibrium does provide an excellent estimation of the abundances of many species, when silicon is exhausted at high density or low entropy. With the small changes in the dominant abundances seen following freezeout of the QSE, methods which employ QSE to reduce the size of the nuclear network should prove reliable for calculation of normal freezeout.

#### 4. $\alpha$ -rich Freezeout

The final test is then to examine the case of silicon exhaustion at low density, which previous authors have dubbed  *$\alpha$ -rich freezeout*. We consider an example of our model for explosive silicon burning, with  $T_{9i} = 6$ ,  $\rho_i = 10^7 \text{ g cm}^{-3}$ , and  $Y_e = .498$ . While at early times the silicon and iron peak groups are separate, by an elapsed time of  $2.9 \times 10^{-7}$  seconds, the abundances of these groups are with 15% of mutual equilibrium. While significant nucleosynthesis has occurred to this point, silicon is far from exhaustion, with a silicon group mass fraction of 65% compared to 11% of the mass being found among the iron peak nuclei. As Figure 5a shows, the light QSE group, which at this point contains more than 13% of the nuclear mass fraction, is more than 5 orders of magnitude underabundant for equilibrium with this combined QSE group. By the time  $1.5 \times 10^{-4}$  seconds have elapsed, the light group, which now represents 36% of the mass, has converged considerably toward equilibrium with this large QSE group, with the network abundance of the light nuclei almost 30% of that required for quasi-equilibrium with  $^{28}\text{Si}$ . The combined silicon and iron peak group is extremely well equilibrated at this time, with only a 4% spread separating germanium from quasi-equilibrium with silicon. Comparison with abundances predicted by NSE, shown in Fig. 6a, reveals that these nuclei are also reasonably close to NSE, with the network abundance of  $^{28}\text{Si}$  being twice its NSE value. The nuclei of the light and Si-Fe QSE groups do show a relatively large spread in abundance when compared to NSE. This spread and the tilt downward with increasing atomic mass shown in this figure are ascribable to a slight underabundance of free protons and  $\alpha$ -particles.

As the expansion and cooling continues, this underabundance of light nuclei reverses. By the time  $2.9 \times 10^{-3}$  seconds have elapsed, with  $T_9$  now 5.96 and  $\rho = 9.8 \times 10^6 \text{ g cm}^{-3}$ , the abundances of the light group nuclei exceed their silicon quasi-equilibrium abundance by 50%. Indeed, the abundances of most of the nuclei lighter than neon exceed their silicon

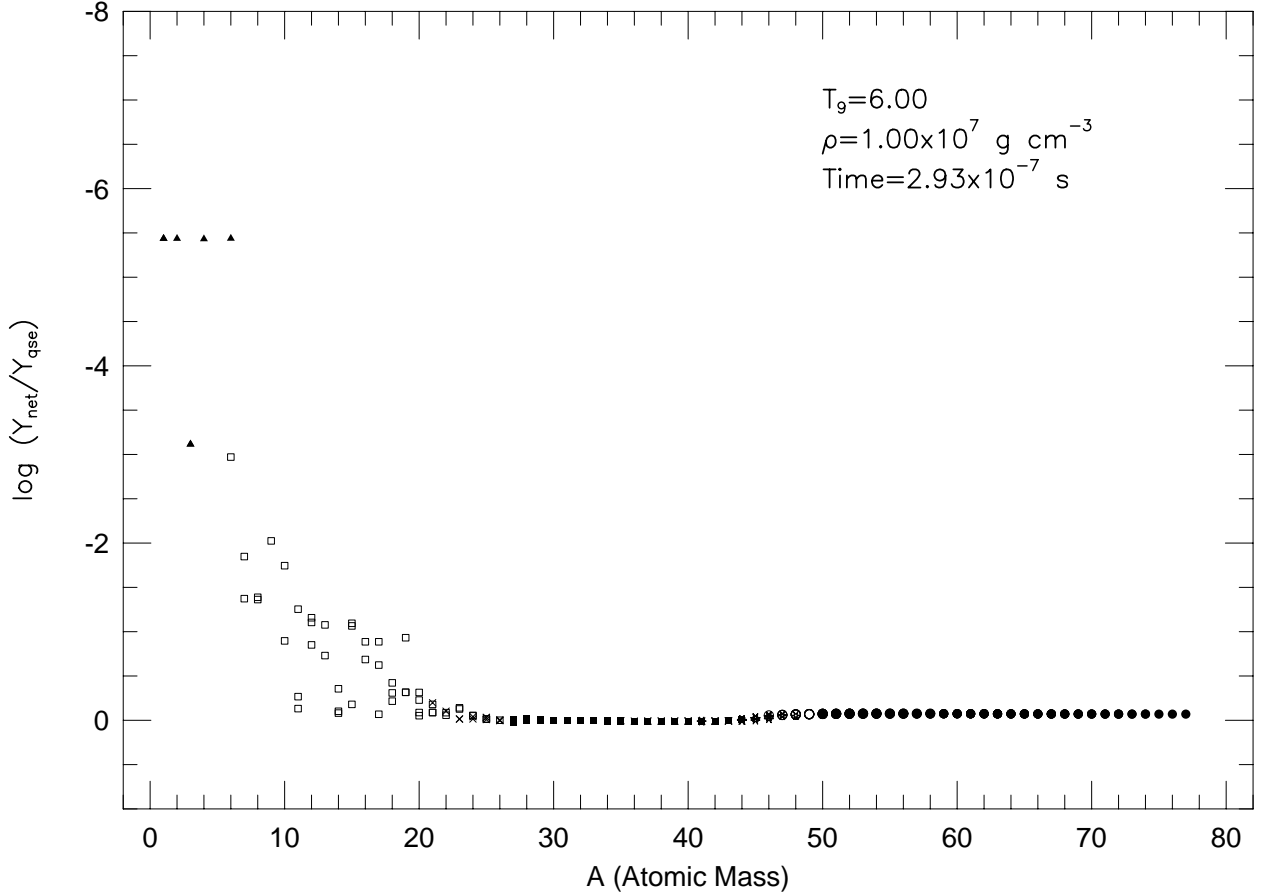


Fig. 5.— (a) Examination of the QSE group structure for  $T_{9i} = 6$ ,  $\rho_i = 10^7 \text{ g cm}^{-3}$ , and  $Y_e = .498$ , after elapsed time of  $2.9 \times 10^{-7}$  seconds.  $Y_{net}$  are the network abundances, while  $Y_{qse}$  are abundances calculated assuming QSE from the network abundances of n, p,  $^{28}\text{Si}$ .

quasi-equilibrium abundance, being nearly in quasi-equilibrium with the free nucleons. Fig. 6b shows that the abundances of the light nuclei are also quite close to their NSE values, with free neutrons and  $\alpha$ -particles slightly exceeding their NSE abundances. This is the beginning of the  $\alpha$ -rich freezeout, with the light group mass fraction of 38% being 3% larger than NSE predicts. As a result, it is now the more massive members of the iron peak group (which comprises 50% of the mass) whose abundance exceeds their NSE abundance. While the abundances of the nuclei between silicon and germanium display a relatively large 50% spread when compared to NSE, the spread from quasi-equilibrium is only 5%. As the evolution proceeds the free nucleon and  $\alpha$ -particle abundances continue to drop more slowly than NSE would predict. By the time  $T_9 = 5.0$  (elapsed time =  $7.7 \times 10^{-2}$  seconds), the light group mass fraction has dropped to 13%. But for NSE at  $T_9 = 5.0$  and  $\rho = 5.8 \times 10^6 \text{ g cm}^{-3}$ , the light group should contain less than 8% of the mass. As a result,  $\alpha$ -particles have twice their NSE abundance, and the overabundance of the more massive

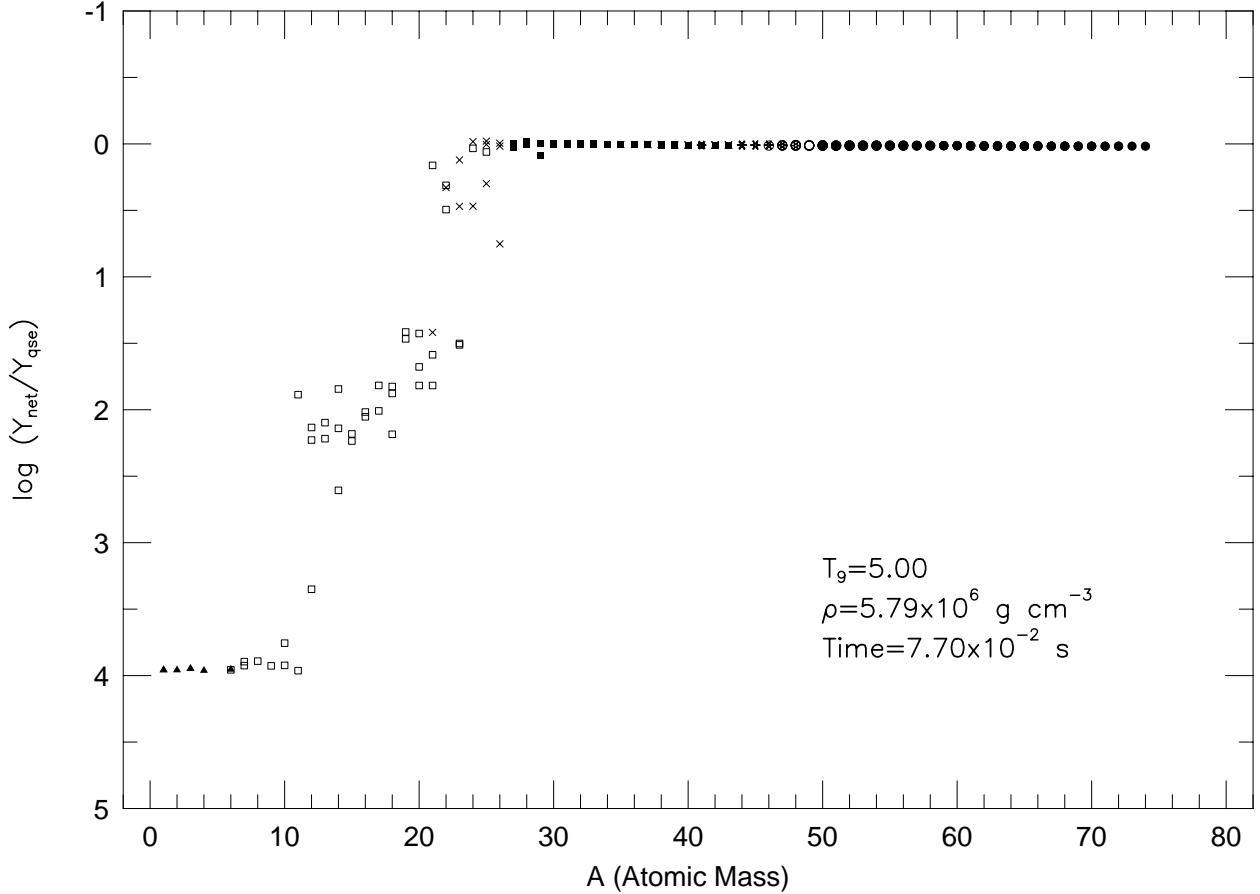


Fig. 5.— (b) Examination of the QSE group structure for  $T_{9i} = 6$ ,  $\rho_i = 10^7 \text{ g cm}^{-3}$ , and  $Y_e = .498$ , after elapsed time of  $7.70 \times 10^{-2}$  seconds ( $T_9 = 5.0$  and  $\rho = 5.8 \times 10^6 \text{ g cm}^{-3}$ ).  $Y_{net}$  are the network abundances, while  $Y_{qse}$  are abundances calculated assuming QSE from the network abundances of n, p,  $^{28}\text{Si}$ .

members of the iron peak group grows. However, as Figure 5b reveals, while the light QSE group has grown 4 orders of magnitude overabundant relative to QSE with silicon, the combined silicon and iron QSE groups remain within 5% of mutual equilibrium.

As time continues to elapse, and temperature continues to drop, the silicon group fragments into several smaller groups and detaches from the iron peak group. The breakdown of this group results from the slow reaction flows from these nuclei which prevent the network abundances of the intermediate nuclei from declining as rapidly as quasi-equilibrium with the iron peak group would require. With the total mass fraction of the former silicon group being a few  $\times 10^{-7}$ , and the light and iron peak QSE groups containing 99.97% of the mass, this breakdown into smaller quasi-equilibrium groups does not strongly affect the overall nuclear evolution. The light and iron peak groups each remain unfragmented, with differences in relative abundance of less than 5%. With the light group

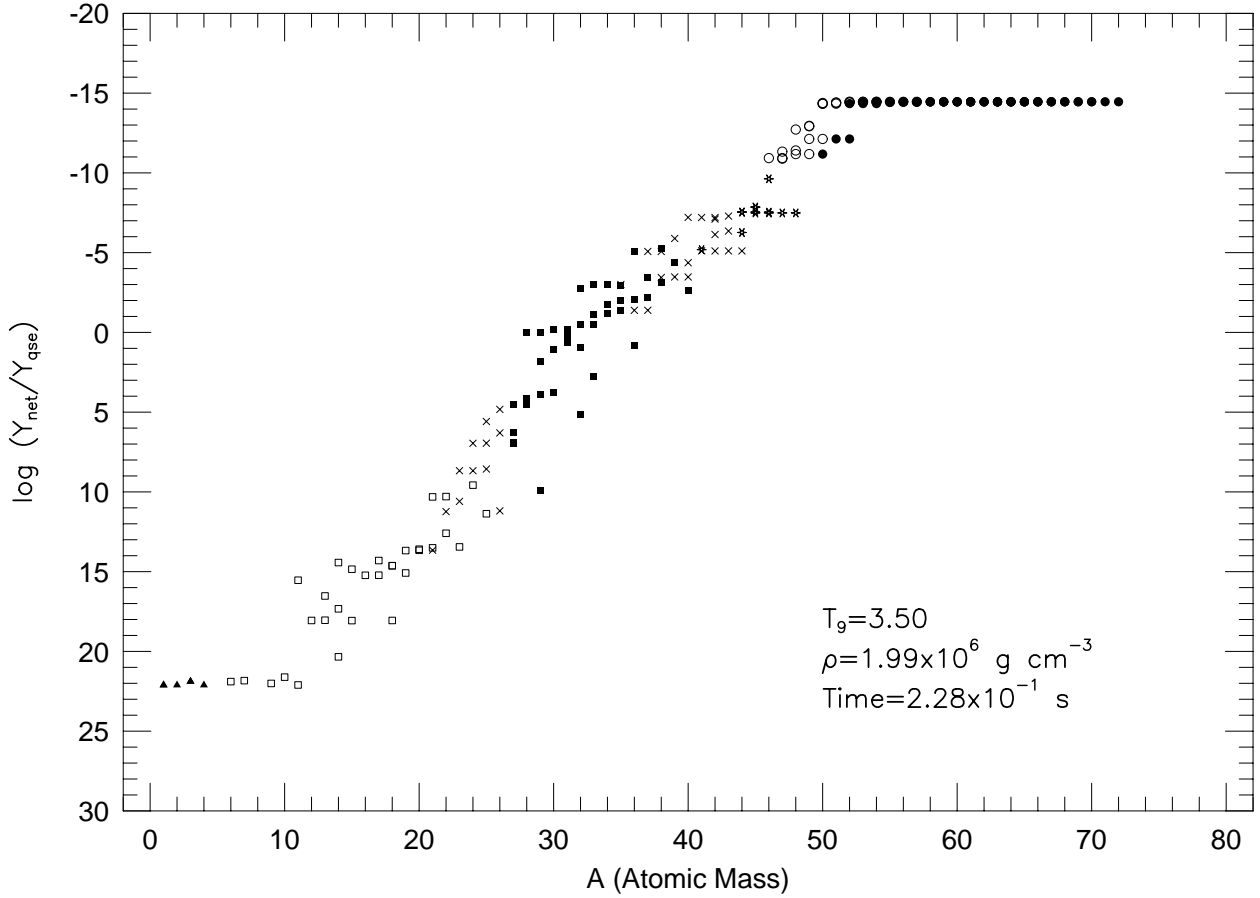


Fig. 5.— (c) Examination of the QSE group structure for  $T_{9i} = 6$ ,  $\rho_i = 10^7 \text{ g cm}^{-3}$ , and  $Y_e = .498$ , after elapsed time of  $2.3 \times 10^{-1}$  seconds ( $T_9 = 3.5$  and  $\rho = 2.0 \times 10^6 \text{ g cm}^{-3}$ ).  $Y_{net}$  are the network abundances, while  $Y_{qse}$  are abundances calculated assuming QSE from the network abundances of n, p,  $^{28}\text{Si}$ .

mass fraction at  $T_9 = 4.0$  almost 17 times its NSE value and the  $\alpha$ -particle abundance more than 35 times that predicted by NSE, the enrichment of the the more massive members of the iron peak group is enormous. As Figure 6c shows, the abundances of the heaviest nuclei contained in our nuclear set, neutron-rich germanium nuclei, like  $^{73}\text{Ge}$  are enhanced 10 million fold over NSE. Among more important nuclei, the abundances of the dominant isotopes of Cu and Zn are enhanced by 100 times, resulting in Cu and Zn mass fractions of .3% and .1%. This behavior is largely consistent with that described by Meyer, Krishnan, & Clayton (1998), who studied the related problem of the cooling of high entropy matter from NSE.

In spite of the large concentration of light nuclei and large departure from NSE, as comparison of columns 2 and 3 of Table 3 demonstrates, the close adherence of the light and iron peak groups to quasi-equilibrium continues as the temperature drops below

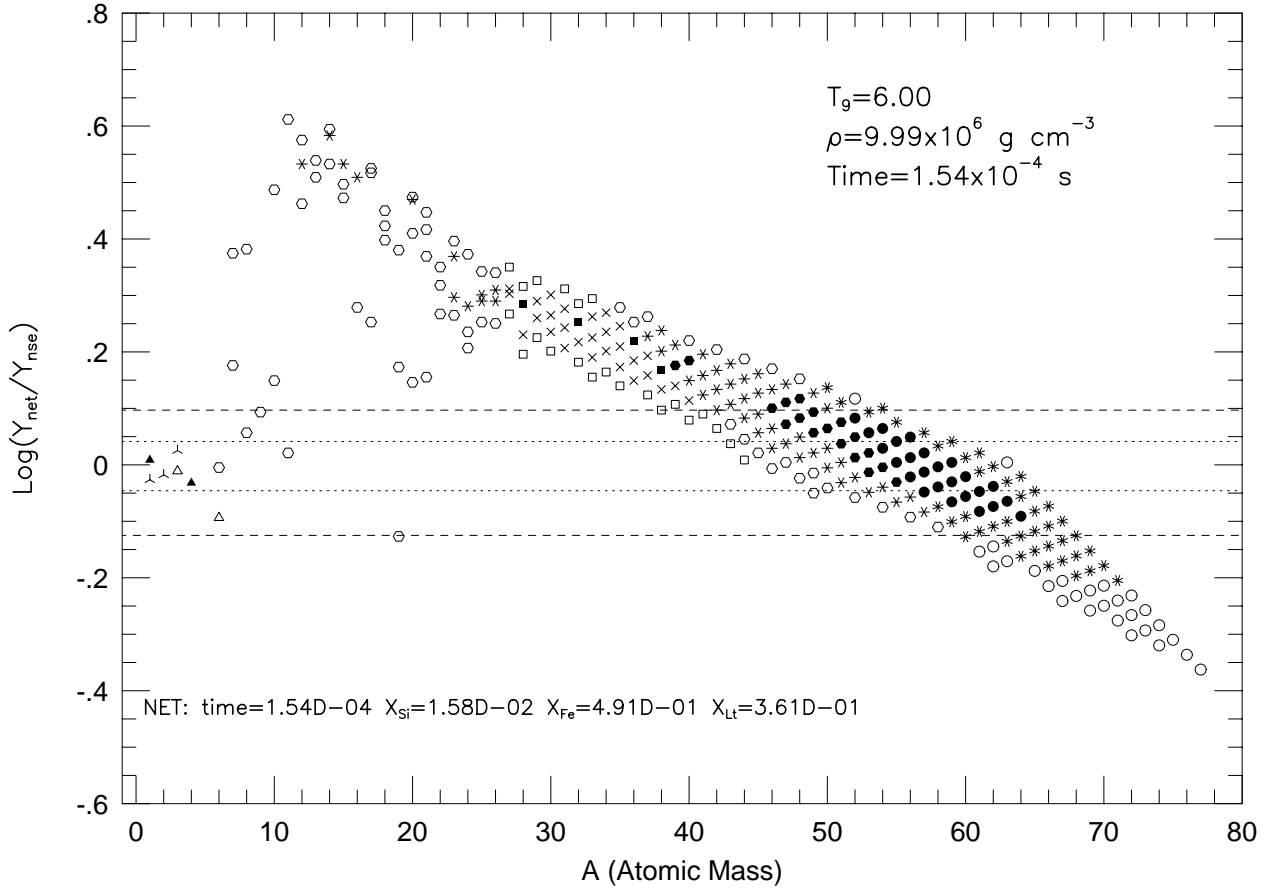


Fig. 6.— (a) Comparison of the network abundances to the NSE abundances for a case with  $T_{9i} = 6$ ,  $\rho_i = 10^7 \text{ g cm}^{-3}$ , and  $Y_e = .498$ , after elapsed times of  $1.54 \times 10^{-4}$  seconds. The filled shapes represent network abundances larger than  $10^{-6}$ , and the hollow shapes denote abundances less than  $10^{-12}$ .

$T_9 = 3.5$ , on its way to freezeout. This differs from the results of Meyer, Krishnan, & Clayton (1998) who claim that QSE breaks down below  $T_9=4$ . Though we agree that the single large QSE group has fragmented, QSE still applies to the groups which dominate the mass fraction and hence it is premature to say QSE has broken down. As Figure 5c shows, these 2 tight QSE groups are linked across more than 30 orders of magnitude difference in quasi-equilibrium by a string of small grouplets with constant  $N$  and individual nuclei. As in the previous cases, the continued decline of temperature toward  $T_9=3$  breaks QSE even within the light and iron peak groups. As comparison of columns 4 and 5 of Table 3 shows, by an elapsed time of .293 seconds, the abundance of  $^4\text{He}$  is 40% smaller than QSE would predict based on the network abundances of free protons and neutrons, with similar errors occurring among the most abundant nuclei in the iron peak group. Unlike previous cases, while the free proton and neutron abundance decline markedly below  $T_9=3.5$ , the large  $\alpha$

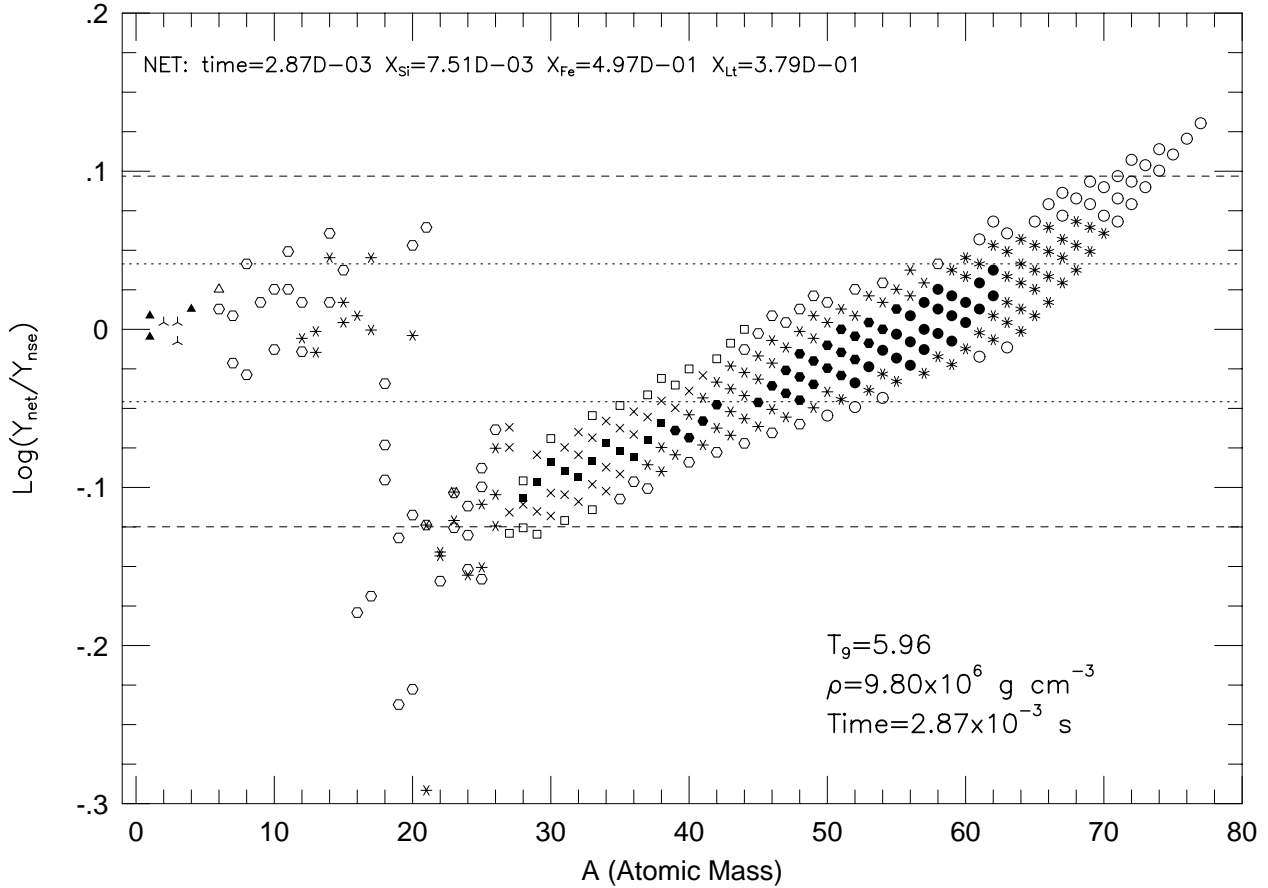


Fig. 6.— (b) Comparison of the network abundances to the NSE abundances for a case with  $T_{9i} = 6$ ,  $\rho_i = 10^7 \text{ g cm}^{-3}$ , and  $Y_e = .498$ , after elapsed time of  $2.9 \times 10^{-3}$  seconds ( $T_9 = 5.96$  and  $\rho = 9.8 \times 10^6 \text{ g cm}^{-3}$ ). The filled shapes represent network abundances larger than  $10^{-6}$ , and the hollow shapes denote abundances less than  $10^{-12}$ .

mass fraction (8%) remains virtually unchanged. Within the time allowed by the cooling timescale, even the freezeout of the  $\alpha$  producing photodisintegrations allows for a decline of  $< 5\%$  in the large  $\alpha$  abundance.

Even this small relative change in the large abundance of  $\alpha$ -particles has strong effects on the smaller abundances, like those of such important  $\alpha$ -rich products as copper, zinc and germanium. By the time the  $\alpha$ -capture reactions which create these nuclei cease, represented in column 7 of Table 3 by abundances after an elapsed time of .445 seconds ( $T_9=2.1$  and  $\rho = 4.3 \times 10^5 \text{ g cm}^{-3}$ ), the mass fractions of these species are .17%, 3.8% and .04%, respectively. Only those abundances which are large compared to the decline in  $Y_\alpha$  are unchanged by freezeout. However, since it is these most abundant nuclei which dominate the energetics of nucleosynthesis, QSE (and future QSE based methods) can provide reasonable estimates of the energy release and other bulk nuclear properties

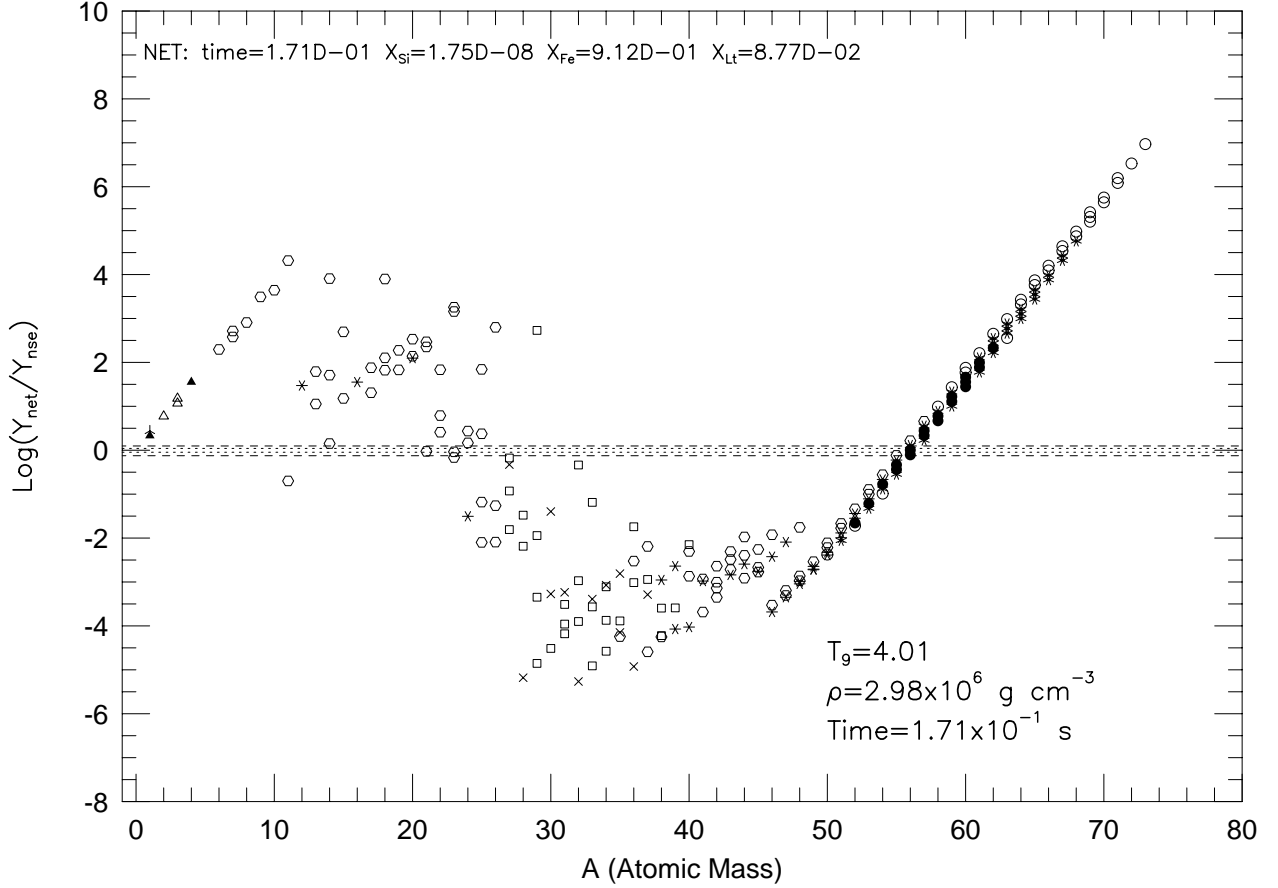


Fig. 6.— (c) Comparison of the network abundances to the NSE abundances for a case with  $T_{9i} = 6$ ,  $\rho_i = 10^7 \text{ g cm}^{-3}$ , and  $Y_e = .498$ , after elapsed time of  $1.7 \times 10^{-1}$  seconds ( $T_9 = 4.0$  and  $\rho = 3.00 \times 10^6 \text{ g cm}^{-3}$ ). The filled shapes represent network abundances larger than  $10^{-6}$ , and the hollow shapes denote abundances less than  $10^{-12}$ .

necessary for accurate hydrodynamic simulations. In addition, though the QSE abundances frozen at  $T_9=3$  (column 5) underestimate the final abundances of the important  $\alpha$ -rich iron peak nuclei by factors of a few to 10, these estimates are much more accurate than the corresponding NSE abundances (column 6). Thus, even in the case of  $\alpha$ -rich freezeout, where its predictions are the least reliable, quasi-equilibrium provides estimates of the nucleosynthesis which are adequate for accurate hydrodynamic modeling and much better than those provided by NSE.



Table 3: Selected abundances near freezeout for the  $\alpha$ -rich freezeout example ( $T_{9i} = 6$ ,  $\rho_1 = 10^7 \text{ g cm}^{-3}$  and  $Y_e = .498$ )

Time	$2.28 \times 10^{-1}$		$2.93 \times 10^{-1}$			$4.45 \times 10^{-1}$
$T_9$	3.50		3.01			2.09
$\rho$	$1.99 \times 10^6$		$1.25 \times 10^6$			$4.25 \times 10^5$
Nucleus	$Y_{net}$	$Y_{qse}$	$Y_{net}$	$Y_{qse}$	$Y_{nse}$	$Y_{net}$
n	$1.94 \times 10^{-12}$	$1.94 \times 10^{-12}$	$5.11 \times 10^{-15}$	$5.11 \times 10^{-15}$	$1.91 \times 10^{-15}$	$2.45 \times 10^{-17}$
p	$2.60 \times 10^{-3}$	$2.60 \times 10^{-3}$	$7.15 \times 10^{-4}$	$7.15 \times 10^{-4}$	$1.48 \times 10^{-5}$	$3.56 \times 10^{-6}$
$^4\text{He}$	$2.05 \times 10^{-2}$	$2.04 \times 10^{-2}$	$2.05 \times 10^{-2}$	$3.27 \times 10^{-2}$	$1.96 \times 10^{-6}$	$1.99 \times 10^{-2}$
$^{28}\text{Si}$	$2.20 \times 10^{-10}$	$2.20 \times 10^{-10}$	$6.10 \times 10^{-10}$	$6.10 \times 10^{-10}$	$9.15 \times 10^{-8}$	$5.13 \times 10^{-9}$
$^{30}\text{Si}$	$3.91 \times 10^{-12}$	$6.44 \times 10^{-16}$	$1.61 \times 10^{-11}$	$2.95 \times 10^{-16}$	$6.16 \times 10^{-15}$	$2.81 \times 10^{-9}$
$^{32}\text{S}$	$3.91 \times 10^{-10}$	$2.31 \times 10^{-7}$	$1.43 \times 10^{-9}$	$3.80 \times 10^{-5}$	$3.41 \times 10^{-7}$	$3.29 \times 10^{-8}$
$^{34}\text{S}$	$3.19 \times 10^{-13}$	$1.71 \times 10^{-11}$	$1.34 \times 10^{-12}$	$7.96 \times 10^{-10}$	$9.95 \times 10^{-13}$	$2.03 \times 10^{-9}$
$^{36}\text{Ar}$	$7.39 \times 10^{-10}$	$8.80 \times 10^{-5}$	$4.08 \times 10^{-9}$	$7.16 \times 10^{-1}$	$3.84 \times 10^{-7}$	$2.83 \times 10^{-7}$
$^{38}\text{Ar}$	$2.42 \times 10^{-13}$	$4.18 \times 10^{-8}$	$6.62 \times 10^{-13}$	$1.32 \times 10^{-4}$	$9.91 \times 10^{-12}$	$6.83 \times 10^{-10}$
$^{40}\text{Ca}$	$7.57 \times 10^{-9}$	$1.23 \times 10^{-1}$	$2.24 \times 10^{-8}$	$6.27 \times 10^{-4}$	$2.01 \times 10^{-6}$	$9.84 \times 10^{-7}$
$^{42}\text{Ca}$	$3.60 \times 10^{-13}$	$4.55 \times 10^{-6}$	$5.12 \times 10^{-13}$	$5.73 \times 10^{-1}$	$2.56 \times 10^{-12}$	$2.86 \times 10^{-10}$
$^{46}\text{Ti}$	$2.25 \times 10^{-12}$	$6.72 \times 10^{-16}$	$1.50 \times 10^{-12}$	$8.47 \times 10^{-22}$	$6.29 \times 10^{-10}$	$1.34 \times 10^{-11}$
$^{48}\text{Ti}$	$1.09 \times 10^{-17}$	$2.00 \times 10^{-19}$	$3.98 \times 10^{-19}$	$9.31 \times 10^{-26}$	$9.63 \times 10^{-15}$	$2.72 \times 10^{-16}$
$^{54}\text{Fe}$	$1.59 \times 10^{-5}$	$1.60 \times 10^{-5}$	$4.13 \times 10^{-7}$	$4.14 \times 10^{-7}$	$1.10 \times 10^{-3}$	$2.38 \times 10^{-10}$
$^{56}\text{Fe}$	$6.07 \times 10^{-9}$	$6.10 \times 10^{-9}$	$3.36 \times 10^{-11}$	$5.33 \times 10^{-11}$	$1.97 \times 10^{-8}$	$3.31 \times 10^{-13}$
$^{58}\text{Fe}$	$1.78 \times 10^{-16}$	$1.79 \times 10^{-16}$	$6.91 \times 10^{-20}$	$1.17 \times 10^{-19}$	$6.02 \times 10^{-18}$	$2.22 \times 10^{-19}$
$^{56}\text{Ni}$	$1.24 \times 10^{-2}$	$1.24 \times 10^{-2}$	$1.35 \times 10^{-2}$	$1.35 \times 10^{-2}$	$1.54 \times 10^{-2}$	$1.36 \times 10^{-2}$
$^{58}\text{Ni}$	$2.67 \times 10^{-3}$	$2.68 \times 10^{-3}$	$1.92 \times 10^{-3}$	$3.07 \times 10^{-3}$	$4.86 \times 10^{-4}$	$1.43 \times 10^{-3}$
$^{60}\text{Ni}$	$5.79 \times 10^{-7}$	$5.82 \times 10^{-7}$	$8.53 \times 10^{-8}$	$2.22 \times 10^{-7}$	$4.89 \times 10^{-9}$	$6.67 \times 10^{-10}$
$^{60}\text{Zn}$	$1.21 \times 10^{-5}$	$1.21 \times 10^{-5}$	$4.41 \times 10^{-5}$	$7.04 \times 10^{-5}$	$4.77 \times 10^{-9}$	$3.67 \times 10^{-4}$
$^{62}\text{Zn}$	$2.34 \times 10^{-5}$	$2.35 \times 10^{-5}$	$7.91 \times 10^{-5}$	$2.06 \times 10^{-4}$	$1.94 \times 10^{-9}$	$2.34 \times 10^{-4}$
$^{64}\text{Zn}$	$3.35 \times 10^{-8}$	$3.37 \times 10^{-8}$	$3.30 \times 10^{-8}$	$1.40 \times 10^{-7}$	$1.84 \times 10^{-13}$	$3.14 \times 10^{-9}$

## 5. Conclusions

Through these examples we have demonstrated that quasi-equilibrium continues to be a useful approximation during silicon burning even when the thermodynamic gradients are strong. Provided there is sufficient abundance within a QSE groups, adjustments within the group happen much faster than reactions outside of these groups. Furthermore these adjustments occur on the timescales of the unbalanced reactions, much more rapidly than reasonable thermodynamic variations. In a recent paper (Hix, Khokhlov, Wheeler & Thielemann 1998), we discuss methods which use QSE to reduce the computational load of silicon burning, while retaining the necessary accuracy, for the limited case of  $\alpha$ -chain nucleosynthesis. For relatively low temperatures, or fast expansions, conditions which result

in the incomplete burning of silicon, quasi-equilibrium holds for temperatures exceeding approximately  $3 \times 10^9$  Kelvins. Below this temperature, differential freezeout of reactions breaks up the large quasi-equilibrium groups but does not result in significant changes to the dominant abundances. For conditions where temperature and density are sufficient to exhaust silicon, but the expansion occurs too rapidly for the complete incorporation of light nuclei into iron peak nuclei to occur,  *$\alpha$ -rich freezeout* occurs. The resultant overabundance of  $\alpha$ -particles and free nucleons obeys quasi-equilibrium, as does the enhancement of more massive iron peak nuclei. Quasi-equilibrium fails in the vicinity of silicon once silicon is exhausted, but the light and iron peak groups which dominate the nuclear evolution continue to obey quasi-equilibrium until the temperature drops to roughly  $3 \times 10^9$  Kelvins. Though the continued capture of the large abundances of light nuclei does result in significant abundance changes, predictions of abundance based on QSE provide good estimates of the largest abundances and hence the energetics and are significantly more reliable than those based on NSE. For expansion which occurs more slowly, previous authors have contended that silicon burned quickly to NSE, and that subsequently the nuclear distribution smoothly followed NSE until the NSE froze out at roughly  $T_9 = 3$ . We have found that while the abundances of the dominant nuclei, the iron peak nuclei, free nucleons and  $\alpha$ -particles, do follow NSE rather smoothly, the intermediate nuclei, carbon, oxygen, and silicon, for example, lag behind. As a result the abundances of these nuclei can be enhanced by several orders of magnitude at freezeout. More importantly for our purposes, though NSE fails to properly account for these abundances, quasi-equilibrium remains an accurate estimate for these as well as the more important nuclei. Thus quasi-equilibrium provides estimates of abundances as accurate or more accurate than NSE, even in the case of the *normal freezeout*. Taken together, we see that even for simulations which include strong thermodynamic gradients, quasi-equilibrium reliably provides good estimates of the abundances of many nuclear species resulting from silicon burning, and will be a valuable tool as we investigate the nucleosynthesis predictions of multi-dimensional supernovae simulations.

The authors would like to thank B.S. Meyer, C. Freiburghaus, K. Nomoto, J.C. Wheeler, and A.G.W. Cameron for fruitful discussions. They would also like to thank the Institute of Theoretical Physics at the University of California, Santa Barbara, for its hospitality and support under NSF grant No. PHY94-07194. Work done at the Oak Ridge National Laboratory was supported by the U.S. Department of Energy under contract DE-FG02-96ER40983 (Joint Institute for Heavy Ion Research) and DE-AC05-96OR22464 (with Lockheed Martin Energy Research Corp). WRH was also supported in part by NASA Grant NAG5-2888. FKT was supported in part by Swiss Nationalfonds grant 20-47252.96

## REFERENCES

- Bazan, G., & Arnett, W.D. 1994, *ApJ*, 433, L41
- Bodansky, D., Clayton, D.D., & Fowler, W.A. 1968, *ApJS*, 16, 299
- Burbidge, E.M., Burbidge, G.R., Fowler, A.A., & Hoyle, F. 1957, *Rev. Mod. Phys.*, 29, 547
- Burrows, A., Hayes, J. & Fryxell, B.A. 1995, *ApJ*, 450, 830
- Clayton, D.D. 1968, 1983, *Principles of Stellar Evolution and Nucleosynthesis*,  
(Chicago:Univ. of Chicago)
- Clifford, F.E., & Tayler, R.J. 1965, *MmRAS*, 69, 21
- Fowler, W.A., & Hoyle, F. 1964, *ApJS*, 9, 201
- Hartmann, D., Woosley, S.E., & El Eid, M.F. 1985, *ApJ*, 297, 837
- Hix, W.R., & Thielemann F.-K. 1996, *ApJ*, 460, 869
- Hix, W.R., Thielemann F.-K., Fushiki, I. & Truran, J.W. 1999, *ApJ*, submitted
- Hix, W.R., Khokhlov, A.M., Wheeler, J.C. & Thielemann F.-K. 1998, *ApJ*, 503, 332
- Herant, M., Benz, W., Hix, W. R., Fryer, C.L., Colgate, S. A. 1994, *ApJ*, 435, 339
- Janka, H.T. & Müller, E. 1995, *ApJ*, 448, L109
- Khokhlov, A.M. 1993, *ApJ*, 419, 200
- Khokhlov, A.M. 1995, *ApJ*, 449, 695
- Meyer, B.S., Krishnan, T.D., & Clayton, D.D. 1996, *ApJ*, 462, 825
- Meyer, B.S., Krishnan, T.D., & Clayton, D.D. 1998, *ApJ*, 498, 808
- Mezzacappa, A., Calder, A.C., Bruenn, S.W., Blondin, J.M., Guidry, M.W., Strayer, M.R.,  
Umar, A.S. 1998, *ApJ*, in press
- Niemeyer, J.C., & Hillebrandt, W. 1995, *ApJ*, 452, 769
- Thielemann, F.-K., Nomoto, K., Yokoi, K. 1986, *A&A*, 158 17
- Thielemann, F.-K., Nomoto, K., Hashimoto, M. 1996, *ApJ*, 460 408
- Truran, J.W., Cameron, A.G.W., & Gilbert, A. 1966, *Can. J. Phys.*, 44, 563
- Woosley, S.E., Arnett, W.D., & Clayton, D.D. 1973, *ApJS*, 26, 231
- Woosley, S.E., Weaver, T.A. 1995, *ApJS*, 101, 181